



CERN-EP-2021-145
18 July 2021

Measurements of the groomed and ungroomed jet angularities in pp collisions at $\sqrt{s} = 5.02$ TeV

ALICE Collaboration*

Abstract

The jet angularities are a class of jet substructure observables which characterize the angular and momentum distribution of particles within jets. These observables are sensitive to momentum scales ranging from perturbative hard scatterings to nonperturbative fragmentation into final-state hadrons. We report measurements of several groomed and ungroomed jet angularities in pp collisions at $\sqrt{s} = 5.02$ TeV with the ALICE detector. Jets are reconstructed using charged particle tracks at midrapidity ($|\eta| < 0.9$). The anti- k_T algorithm is used with jet resolution parameters $R = 0.2$ and $R = 0.4$ for several transverse momentum $p_T^{\text{ch jet}}$ intervals in the 20–100 GeV/c range. Using the jet grooming algorithm Soft Drop, the sensitivity to softer, wide-angle processes, as well as the underlying event, can be reduced in a way which is well-controlled in theoretical calculations. We report the ungroomed jet angularities, λ_α , and groomed jet angularities, $\lambda_{\alpha,g}$, to investigate the interplay between perturbative and nonperturbative effects at low jet momenta. Various angular exponent parameters $\alpha = 1, 1.5, 2, \text{ and } 3$ are used to systematically vary the sensitivity of the observable to collinear and soft radiation. Results are compared to analytical predictions at next-to-leading-logarithmic accuracy, which provide a generally good description of the data in the perturbative regime but exhibit discrepancies in the nonperturbative regime. Moreover, these measurements serve as a baseline for future ones in heavy-ion collisions by providing new insight into the interplay between perturbative and nonperturbative effects in the angular and momentum substructure of jets. They supply crucial guidance on the selection of jet resolution parameter, jet transverse momentum, and angular scaling variable for jet quenching studies.

arXiv:2107.11303v2 [nucl-ex] 1 Dec 2022

© 2021 CERN for the benefit of the ALICE Collaboration.

Reproduction of this article or parts of it is allowed as specified in the CC-BY-4.0 license.

*See Appendix B for the list of collaboration members

1 Introduction

In high-energy particle collisions, jet observables are sensitive to a variety of processes in quantum chromodynamics (QCD), from the initial hard (high Q^2) parton scattering to a scale evolution culminating in hadronization near Λ_{QCD} . Jets reconstructed with a radius (resolution) parameter near $R = 1$ and with sufficiently large transverse momentum $p_{\text{T}}^{\text{jet}}$ provide a proxy for the dynamics of the initial hard parton scattering, whereas those reconstructed with smaller R or at lower $p_{\text{T}}^{\text{jet}}$ become sensitive to nonperturbative effects. In this article, jet substructure observables are defined by clustering particles into a jet and then constructing an observable from its constituents to characterize its internal radiation pattern.

Jet substructure techniques have provided one of the key tools to study rare event topologies in pp collisions, for example by tagging boosted objects that decay into jets [1]. Moreover, measurements of jet substructure enable stringent tests of perturbative QCD (pQCD) and facilitate studies of nonperturbative effects which are not yet under satisfactory theoretical control [2]. Jet substructure observables offer both flexibility and rigor: they can be constructed to be theoretically calculable from first-principles pQCD while simultaneously maintaining sensitivity to jet radiation in specific regions of phase-space. Jet grooming algorithms, such as Soft Drop [3–5], can additionally be used to remove soft, wide-angle radiation via well-controlled approaches, reducing nonperturbative effects. This defines two families of jet substructure observables: one that can be constructed from all jet constituents and one based on a subset of jet constituents which remain after grooming procedures.

One such set of observables are the generalized jet angularities [6, 7]. Expanding upon the jet girth g (also known as the jet radial moment), the generalized jet angularities form a class of jet substructure observables defined by

$$\lambda_{\alpha}^{\kappa} \equiv \sum_i z_i^{\kappa} \theta_i^{\alpha}, \quad (1)$$

where the sum runs over the jet constituents i , and κ and α are continuous free parameters.¹ The first factor $z_i \equiv p_{\text{T},i}/p_{\text{T}}^{\text{jet}}$ describes the momentum fraction carried by the constituent, and the second factor $\theta_i \equiv \Delta R_i/R$ denotes the separation in rapidity (y) and azimuthal angle (φ) of the constituent from the jet axis, where $\Delta R_i \equiv \sqrt{\Delta y_i^2 + \Delta \varphi_i^2}$ and R is the jet resolution parameter. The jet angularities are infrared- and collinear- (IRC-)safe for $\kappa = 1$ and $\alpha > 0$ [8, 9]. We consider the ungroomed jet angularities, denoted as λ_{α} , as well as the groomed jet angularities in which the sum runs only over the constituents of the groomed jet, denoted as $\lambda_{\alpha,g}$. These include the jet girth [10], λ_1 , and the jet thrust [11], λ_2 , which is related to the jet mass m_{jet} by $\lambda_2 = (m_{\text{jet}}/p_{\text{T}}^{\text{jet}})^2 + \mathcal{O}(\lambda_2^2)$; λ_2 , however, is more robust against nonperturbative effects than m_{jet} since it does not depend explicitly on the hadron masses.

The IRC-safe jet angularities offer the possibility to systematically vary the observable definition in a way that is theoretically calculable and therefore provide a rich opportunity to study both perturbative and nonperturbative QCD [12–15]. This article considers jet angularities constructed from charged-particle jets. While charged-particle jets are IRC-unsafe [16], comparisons to these theoretical predictions can nonetheless be carried out by following a nonperturbative correction procedure, as outlined in Sec. 5.1. Jet angularities were recently calculated in pp collisions both in the ungroomed [9] and groomed [17] cases, as well as for jets produced in association with a Z boson [18]. These calculations use all-order resummation of large logarithms up to next-to-leading-logarithmic (NLL') accuracy [19]. Measurements of λ_{α} and $\lambda_{\alpha,g}$ will serve to test these analytical predictions, in particular the role of resummation effects and power corrections. Moreover, by measuring multiple values of α , one can test the predicted scaling of nonperturbative shape functions that are used to model hadronization, which depend only on a single

¹The notation λ_{α} is employed to represent the jet angularities instead of the commonly-used notation λ_{β} in order to avoid conflict with the letter β , which is also used to denote the angular parameter of the Soft Drop grooming algorithm.

nonperturbative parameter for all values of α [20, 21].

Several measurements of jet angularities have been performed in hadronic collisions. The ungroomed jet angularity λ_1 has been measured in pp collisions by the ATLAS, CMS, and ALICE Collaborations [22–24] in addition to $p\bar{p}$ collisions by the CDF Collaboration [25]. The ungroomed jet angularity λ_2 has also been measured in pp collisions by the CMS Collaboration [24]. The closely related ungroomed and groomed jet mass have been extensively measured in pp collisions by the ATLAS and CMS Collaborations [23, 24, 26–35], and the ungroomed mass was also studied in $p\bar{p}$ collisions by the CDF Collaboration [25] and in p–Pb collisions by the ALICE Collaboration [36]. Many of these measurements have focused on using jet substructure for tagging objects at high p_T , rather than for fundamental studies of QCD, and with the exception of the jet mass there have not yet been comparisons of jet angularities to analytical calculations, nor have any such comparisons been made for charged-particle jets. In this article, we perform the first measurements of groomed jet angularities in pp collisions, and a systematic scan of the IRC-safe ungroomed jet angularities. These measurements focus on low to moderate p_T^{jet} , and small to moderate R . Moreover, the measurements are performed in pp collisions at a center-of-mass energy $\sqrt{s} = 5.02$ TeV, the same center-of-mass energy at which ALICE recorded data in heavy-ion collisions during LHC Run 2, and where no jet angularity measurements have been made.

These measurements serve as a baseline for future measurements of the jet angularities in heavy-ion collisions, in which a deconfined state of strongly-interacting matter is produced [37–40]. Measurements of jets and jet substructure in heavy-ion collisions may provide key insight into the physical properties of this deconfined state [41–43]. The jet angularities are sensitive both to medium-induced broadening as well as jet collimation [44–46]; by systematically varying the weight of collinear radiation, one may be able to efficiently discriminate between jet quenching models. In Pb–Pb collisions, λ_1 has been measured for $R = 0.2$ by the ALICE Collaboration [22], and the ungroomed and groomed jet mass have been measured for $R = 0.4$ by the ATLAS, CMS, and ALICE Collaborations [30, 34, 36]. The interpretation of previous measurements is unclear, with strong modification being observed in Pb–Pb collisions compared to pp collisions for the case when $\alpha = 1$ and $R = 0.2$, but little to no modification seen for the $R = 0.4$ jet mass. Future measurements over a range of R and α offer a compelling opportunity to disentangle the roles of medium-induced broadening, jet collimation, and medium response in jet evolution. By measuring small to moderate R jets in pp collisions, which are theoretically challenging and involve significant resummation effects [47], the ability of pQCD to describe the small-radius jets that are measured in heavy-ion collisions can be tested.

This article reports measurements of ungroomed and groomed jet angularities for $\alpha = 1, 1.5, 2,$ and 3 in pp collisions at $\sqrt{s} = 5.02$ TeV. In addition to the standard jet girth ($\alpha = 1$) and jet mass (related to $\alpha = 2$) parameters, $\alpha = 1.5$ and $\alpha = 3$ are included to test the universality of a nonperturbative shape function by varying effects of soft, wide-angle radiation, as discussed below in Sec. 5.1.2, and to serve as a reference for future jet quenching measurements in heavy-ion collisions. Grooming is performed according to the Soft Drop grooming procedure with $z_{\text{cut}} = 0.2$ and $\beta = 0$ [48]. Charged particle jets were reconstructed at midrapidity using the anti- k_T algorithm with jet resolution (radius) parameters $R = 0.2$ and $R = 0.4$ in four equally-sized $p_T^{\text{ch,jet}}$ intervals from 20 to 100 GeV/ c . The results are compared to NLL' pQCD predictions, as well as to the PYTHIA8 [49] and Herwig7 [50, 51] Monte Carlo generators.

2 Experimental setup and data sets

A description of the ALICE detector and its performance can be found in Refs. [52, 53]. The pp data used in this analysis were collected in 2017 during LHC Run 2 at $\sqrt{s} = 5.02$ TeV [54]. A minimum bias (MB) trigger was used; this requires a coincidence of hits in the V0 scintillator detectors, which provide full azimuthal coverage and cover the pseudorapidity ranges of $2.8 < \eta < 5.1$ and $-3.7 < \eta < -1.7$ [55]. The event selection also requires the location of the primary vertex to be within ± 10 cm from the nom-

inal interaction point (IP) along the beam direction and within 1 cm of the IP in the transverse plane. Beam-induced background events were removed using two neutron Zero Degree Calorimeters located at ± 112.5 m along the beam axis from the center of the detector. Events with multiple reconstructed vertices were rejected, and track quality selection criteria ensured that tracks used in the analysis were from only one vertex. Events were acquired at instantaneous luminosities between approximately 10^{30} and 10^{31} $\text{cm}^{-2}\text{s}^{-1}$, corresponding to a low level of pileup with approximately $0.004 < \mu < 0.03$ events per bunch crossing. The pp data sample contains 870 million events and corresponds to an integrated luminosity of $18.0(4)$ nb^{-1} [56].

This analysis uses charged particle tracks reconstructed from clusters in both the Time Projection Chamber (TPC) [57] and the Inner Tracking System (ITS) [58]. Two types of tracks are defined: global tracks and complementary tracks. Global tracks are required to include at least one hit in the silicon pixel detector (SPD), comprising the first two layers of the ITS, and to satisfy a number of quality criteria [59], including having at least 70 out of a maximum of 159 TPC space points and at least 80% of the geometrically findable space points in the TPC. Complementary tracks do not contain any hits in the SPD, but otherwise satisfy the tracking criteria, and are refit with a constraint to the primary vertex of the event. Including this second class of tracks ensures approximately uniform azimuthal acceptance, while preserving similar transverse momentum p_T resolution to tracks with SPD hits, as determined from the fit quality. Tracks with $p_{T,\text{track}} > 0.15$ GeV/c are accepted over pseudorapidity $|\eta| < 0.9$ and azimuthal angle $0 < \varphi < 2\pi$. All tracks are assigned a mass equal to the π^\pm mass.

The instrumental performance of the ALICE detector and its response to particles is estimated with a GEANT3 [60] model. The tracking efficiency in pp collisions, as estimated by propagating pp events from PYTHIA8 Monash 2013 [49] through the ALICE GEANT3 detector simulation, is approximately 67% at $p_{T,\text{track}} = 0.15$ GeV/c , rises to approximately 84% at $p_{T,\text{track}} = 1$ GeV/c , and remains above 75% at higher p_T . The momentum resolution $\sigma(p_T)/p_T$ is estimated from the covariance matrix of the track fit [53] and is approximately 1% at $p_{T,\text{track}} = 1$ GeV/c . This increases with $p_{T,\text{track}}$, reaching approximately 4% at $p_{T,\text{track}} = 50$ GeV/c .

3 Analysis method

3.1 Jet reconstruction

Jets are reconstructed from charged tracks with $p_T > 150$ MeV/c using the FastJet package [61]. The anti- k_T algorithm is used with the E recombination scheme for resolution parameters $R = 0.2$ and 0.4 [62]. All reconstructed charged-particle jets in the transverse momentum range $5 < p_T^{\text{ch jet}} < 200$ GeV/c are analyzed in order to maximize statistics in the unfolding procedure (described below). Each jet axis is required to be within the fiducial volume of the TPC, $|\eta_{\text{jet}}| < 0.9 - R$. Jets containing a track with $p_T > 100$ GeV/c are removed from the collected data sample, due to limited momentum resolution. In order to make consistent comparisons between the data and the theoretical calculations, the background due to the underlying event is not subtracted from the data, and instead the underlying event (along with other nonperturbative effects) is included in model corrections, as described in Sec. 5.1.

The jet reconstruction performance is studied by comparing jets reconstructed from PYTHIA8-generated events at “truth level” (before the particles undergo interactions with the detector) to those at “detector level” (after the ALICE GEANT3 detector simulation). Two collections of jets are constructed: pp truth level (PYTHIA truth) and pp detector level (PYTHIA with detector simulation). The detector-level jets are then geometrically matched with truth-level jets within $\Delta R < 0.6 R$ while additionally requiring that each match be unique. Table 1 shows approximate values of the mean jet energy scale shift, $\Delta_{\text{JES}} = \left\langle \left(p_{T,\text{det}}^{\text{ch jet}} - p_{T,\text{truth}}^{\text{ch jet}} \right) / p_{T,\text{truth}}^{\text{ch jet}} \right\rangle$, the jet energy resolution, $\text{JER} = \sigma \left(p_{T,\text{det}}^{\text{ch jet}} \right) / p_{T,\text{truth}}^{\text{ch jet}}$, and the jet reconstruction efficiency, ϵ_{reco} , for both $R = 0.2$ and $R = 0.4$, where $p_{T,\text{det}}^{\text{ch jet}}$ is the detector-level $p_T^{\text{ch jet}}$,

Table 1: Approximate values characterizing the jet reconstruction performance for $R = 0.2$ and 0.4 in pp collisions. Δ_{JES} is the mean jet energy scale shift, JER is the jet energy resolution, and ϵ_{reco} is the reconstruction efficiency.

$p_{\text{T}}^{\text{ch jet}}$	$R = 0.2$		$R = 0.4$	
	20 GeV/c	100 GeV/c	20 GeV/c	100 GeV/c
Δ_{JES}	-12%	-24%	-13%	-21%
JER	22%	21%	21%	21%
ϵ_{reco}	94%	100%	97%	100

and $p_{\text{T},\text{truth}}^{\text{ch jet}}$ is the truth-level $p_{\text{T}}^{\text{ch jet}}$. The jet energy scale shift is a long-tailed asymmetric distribution due to tracking inefficiency [63] with a peak at $p_{\text{T},\text{det}}^{\text{ch jet}} = p_{\text{T},\text{truth}}^{\text{ch jet}}$, and Δ_{JES} should be understood only as a rough characterization of this distribution.

The ungroomed jet angularities are reconstructed using all of the charged-particle jet constituents according to Eq. (1). For the groomed jet angularities, Soft Drop grooming [3] is performed, in which the constituents of each jet are reclustered with the Cambridge–Aachen algorithm [64] with resolution parameter R , forming an angularly-ordered tree data structure. Each node corresponds to a constituent track, and each edge is a branch splitting defined by $z \equiv \frac{p_{\text{T},\text{subleading}}}{p_{\text{T},\text{leading}} + p_{\text{T},\text{subleading}}}$ and $\theta \equiv \frac{\Delta R}{R} \equiv \frac{\sqrt{\Delta y^2 + \Delta \phi^2}}{R}$. The jet tree is then traversed starting from the largest-angle splitting, and the Soft Drop condition, $z > z_{\text{cut}} \theta^\beta$, is recursively evaluated. Here, z is the subleading branch p_{T} fraction defined above, and z_{cut} and β are tunable, free parameters of the grooming algorithm. For this analysis, $\beta = 0$ is used to maximize the perturbative calculability [17], while $z_{\text{cut}} = 0.2$ is chosen (as opposed to the more common $z_{\text{cut}} = 0.1$) since higher-accuracy branch tagging can be achieved in future heavy-ion collision analyses [48]. If the Soft Drop condition is not satisfied, then the softer subleading branch is discarded and the next splitting in the harder branch is examined in the same way. If, however, the condition is satisfied, then the grooming procedure is concluded, with all remaining constituents defining the groomed jet. The groomed jet angularity is then defined according to Eq. (1) using the groomed jet constituents, but still with the ungroomed $p_{\text{T}}^{\text{ch jet}}$ and ungroomed jet axis to define θ_i , since the groomed jet observable is a property of the original (ungroomed) jet object. Note that while the ungroomed $p_{\text{T}}^{\text{ch jet}}$ is IRC-safe, the groomed $p_{\text{T},\text{g}}^{\text{ch jet}}$ is Sudakov safe [65]. If the jet does not contain a splitting that passes the Soft Drop condition, then the groomed jet contains zero constituents (“untagged”) and does not have a defined groomed jet angularity.

3.2 Corrections

The reconstructed $p_{\text{T}}^{\text{ch jet}}$ and λ_α differ from their true values due to tracking inefficiency, particle–material interactions, and track p_{T} resolution. To account for these effects, PYTHIA8 Monash 2013 [49, 66] and the ALICE GEANT3 detector simulation are used to construct a 4D response matrix that describes the detector response mapping of $p_{\text{T},\text{truth}}^{\text{ch jet}}$ and $\lambda_{\alpha,\text{truth}}$ to $p_{\text{T},\text{det}}^{\text{ch jet}}$ and $\lambda_{\alpha,\text{det}}$, where $p_{\text{T},\text{det}}^{\text{ch jet}}$ and $p_{\text{T},\text{truth}}^{\text{ch jet}}$ are as above, and $\lambda_{\alpha,\text{det}}$ and $\lambda_{\alpha,\text{truth}}$ are the analogous detector- and truth-level λ_α . The truth-level jet was constructed from the charged primary particles of the PYTHIA event, defined as all particles with a mean proper lifetime larger than 1 cm/c, and excluding the decay products of these particles [67].

A 2D unfolding in $p_{\text{T}}^{\text{ch jet}}$ and λ_α is then performed using the iterative Bayesian unfolding algorithm [68, 69] implemented in the RooUnfold package [70] to recover the true jet spectrum at the charged-hadron level. This technique utilizes a “prior” distribution (equivalent to the per-bin MC prediction) as a starting point, before iteratively updating the distribution using Bayes’ theorem in conjunction with the calculated response matrix and measured data (see Refs. [68, 69] for details). Since the jet yield in each reported $p_{\text{T}}^{\text{ch jet}}$ interval varies widely, with higher- $p_{\text{T}}^{\text{ch jet}}$ jets being less probable than lower- $p_{\text{T}}^{\text{ch jet}}$ jets, and since the shape and mean value of the jet angularity distributions also changes with $p_{\text{T}}^{\text{ch jet}}$, a separate 2D unfolding for each reported $p_{\text{T}}^{\text{ch jet}}$ bin is performed in order to optimize the observable binning at both

truth and detector levels, thus ensuring sufficient jet yield is included in the procedure for all distributions while simultaneously maximizing the number of bins for regions of phase space where higher yield is available. The bin migration in all cases is dominated by a strong diagonal mapping in the response matrix coupled with a slight smearing along the $p_{T,\text{truth}}^{\text{ch jet}}$ and $\lambda_{\alpha,\text{truth}}$ axes. The smearing in λ_{α} is roughly symmetric about the diagonal, whereas the smearing in $p_{T}^{\text{ch jet}}$ tends to be skewed towards lower values of $p_{T,\text{truth}}^{\text{ch jet}}$ due to tracking efficiency effects.

In the groomed case, the number of untagged jets in the unfolding procedure is included as an additional bin adjacent to the lower edge of the λ_{α} distributions. This is done so that the unfolding procedure will correct for detector effects on the groomed jet tagging fraction as well as account for bin migration effects for jets which are groomed away at detector-level but not truth-level, or vice versa.

To validate the performance of the unfolding procedure, a set of refolding and closure tests is performed, in which either the response matrix is multiplied by the unfolded data and compared to the original detector-level spectrum, or in which the shape of the input MC spectrum is modified to account for the fact that the actual distribution may be different than the MC input spectrum. The number of iterations, which sets the strength of regularization, is chosen to be the minimal value such that all unfolding tests succeed. This results in the number of iterations being equal to 3 for all distributions. In all cases, closure is achieved compatible with statistical uncertainties.

The distributions after unfolding are corrected for the kinematic efficiency, defined as the efficiency of reconstructing a truth-level jet at a particular $p_{T,\text{truth}}^{\text{ch jet}}$ and $\lambda_{\alpha,\text{truth}}$ value given a reconstructed jet $p_{T,\text{det}}^{\text{ch jet}}$ and $\lambda_{\alpha,\text{det}}$ range. Kinematic inefficiency results from effects including smearing from the Soft Drop threshold and p_T -smearing of the jet out of the selected $p_{T,\text{det}}^{\text{ch jet}}$ range. Any “missed” jets, those jets which exist at truth level but not at detector level, are handled by this kinematic efficiency correction. In this analysis, minimal detector-level cuts are applied, and the kinematic efficiency is therefore greater than 99% in all cases. Since a wide $p_{T,\text{truth}}^{\text{ch jet}}$ range is taken, the effect of “fake” jets, those jets which exist at detector level but not truth level, is taken to be negligible.

4 Systematic uncertainties

The systematic uncertainties in the unfolded results arise from uncertainties in the tracking efficiency and unfolding procedure, as well as the model-dependence of the response matrix, and the track mass assumption. Table 2 summarizes the systematic uncertainty contributions. Each of these sources of uncertainty dominate in certain regions of the measured observables, with the exception of the track mass assumption which is small in all cases. The total systematic uncertainty is taken as the sum in quadrature of the individual uncertainties described below.

The tracking efficiency uncertainty is estimated to be 4% by varying track selection parameters and the ITS–TPC matching requirement. In order to assign a systematic uncertainty to the nominal result, a response matrix is constructed using the same techniques as for the final result except that an additional 4% of tracks are randomly rejected before the jet finding. This response matrix is then used to unfold the distribution in place of the nominal response matrix, and the result is compared to the default result, with the differences in each bin taken as a symmetric uncertainty. This uncertainty constitutes a smaller effect in the groomed jet angularities, where single-particle jets, being the most sensitive to the tracking efficiency, are groomed away by the Soft Drop condition. The uncertainty on the track momentum resolution is a sub-leading effect to the tracking efficiency and is taken to be negligible.

Several variations of the unfolding procedure are performed in order to estimate the systematic uncertainty arising from the unfolding regularization procedure:

1. The number of iterations was varied by ± 2 and the average difference with respect to the nominal

result is taken as the systematic uncertainty.

2. The prior distribution is scaled by a power law in $p_T^{\text{ch jet}}$ and a linear scaling in λ_α , $(p_T^{\text{ch jet}})^{\pm 0.5} \times [1 \pm (\lambda_\alpha - 0.5)]$. The average difference between the result unfolded with this prior and the original is taken as the systematic uncertainty.
3. The binning in λ_α was varied to be slightly finer and coarser than the nominal binning, by combining (splitting) some adjacent bins with low (high) jet yield, or by shifting the bin boundaries to be between the nominal boundaries.
4. The lower and upper bounds in the $p_{T,\text{det}}^{\text{ch jet}}$ range were increased to 10 and decreased to 120 GeV/c, respectively. These values are chosen as reasonable values to estimate sensitivity to truncation effects.

The total unfolding systematic uncertainty is then the standard deviation of the variations, $\sqrt{\sum_{i=1}^N \sigma_i^2}/N$, where $N = 4$ and σ_i is the systematic uncertainty due to a single variation, since they each comprise independent measurements of the same underlying systematic uncertainty in the regularization.

A systematic uncertainty associated with the model-dependent reliance on the Monte Carlo generator which is used to unfold the spectra is included. We construct a fast simulation to parameterize the tracking efficiency and track p_T resolution, and build response matrices using PYTHIA8 Monash 2013 and Herwig7 (default tune) as generators. Even though a full detector simulation using PYTHIA8 has also been generated, a fast simulation is used for this purpose so that there is complete parity between the two generators in the calculation of this systematic uncertainty. This fast simulation provides agreement within $\pm 10\%$ of the full detector simulation for $R = 0.2$ jets, with some larger deviations seen in the tails of the jet angularity distributions for $R = 0.4$ jets. These two response matrices are then used to unfold the measured data, and the differences between the two unfolded results in each interval are taken as a symmetric uncertainty. This uncertainty is most significant at lower $p_T^{\text{ch jet}}$.

In order to assess the uncertainty due to the track mass assumption, K^\pm meson and proton masses are randomly assigned to 13% and 5.5% of tracks, respectively, in both the data and the response matrix. These numbers are chosen from the (approximate) inclusive number of each respective particle measured at midrapidity in pp events by ALICE [71]. Neither the measurement inside the jets nor the $p_T^{\text{ch jet}}$ -dependence are considered, so these numbers are taken to constitute a reasonable maximum uncertainty. The bin-by-bin difference of the unfolded result to the nominal result is taken as a symmetric uncertainty.

5 Results and discussion

We report the λ_α and $\lambda_{\alpha,g}$ distributions for $\alpha = 1, 1.5, 2,$ and 3 in four equally-sized intervals of $p_T^{\text{ch jet}}$ between 20 and 100 GeV/c. The distributions are reported as differential cross sections:

$$\frac{1}{\sigma} \frac{d\sigma}{d\lambda_\alpha} \equiv \frac{1}{N_{\text{jets}}} \frac{dN_{\text{jets}}}{d\lambda_\alpha} \text{ (ungroomed), \quad or \quad } \frac{1}{\sigma_{\text{inc}}} \frac{d\sigma}{d\lambda_{\alpha,g}} \equiv \frac{1}{N_{\text{inc jets}}} \frac{dN_{\text{gr jets}}}{d\lambda_{\alpha,g}} \text{ (groomed), \quad (2)}$$

where N_{jets} is the number of jets within a given $p_T^{\text{ch jet}}$ range and σ is the corresponding cross section. For the groomed case, some jets are removed by the grooming procedure, and therefore two different quantities are defined: $N_{\text{gr jets}}$, the number of jets which have at least one splitting satisfying the Soft Drop condition, and $N_{\text{inc jets}}$, the total number of inclusive jets, with both $N_{\text{gr jets}}$ and $N_{\text{inc jets}}$ being within the given $p_T^{\text{ch jet}}$ range. σ_{inc} is the cross section corresponding to the latter inclusive quantity. For the ungroomed case, $N_{\text{inc jets}} = N_{\text{jets}}$ and $\sigma = \sigma_{\text{inc}}$, so the redundant labels are dropped. It is useful to normalize the groomed differential cross section by the number of inclusive jets since the groomed jet angularities

Table 2: Summary of systematic uncertainties for a representative sample of α , R , and $p_T^{\text{ch jet}}$. A moderately high $60 < p_T^{\text{ch jet}} < 80$ GeV/ c with $R = 0.4$ is chosen to show the variation with α , and two additional rows show the trends with smaller $p_T^{\text{ch jet}}$ and R .

	α	R	$p_T^{\text{ch jet}}$ (GeV/ c)	Relative uncertainty				Total
				Trk. eff.	Unfolding	Generator	Mass hypothesis	
λ_α	1	0.4	60–80	1–15%	2–7%	1–5%	0–2%	7–16%
	2	0.4	60–80	1–10%	1–8%	1–5%	1–3%	4–12%
	3	0.4	60–80	1–10%	2–4%	1–4%	0–4%	4–11%
	2	0.4	20–40	1–16%	1–4%	1–43%	0–5%	2–44%
	2	0.2	60–80	2–12%	2–7%	1–9%	0–2%	3–12%
$\lambda_{\alpha,g}$	1	0.4	60–80	1–7%	2–8%	1–6%	0–4%	2–13%
	2	0.4	60–80	1–8%	2–9%	1–5%	0–4%	3–12%
	3	0.4	60–80	1–6%	2–7%	1–11%	0–7%	4–16%
	2	0.4	20–40	1–8%	2–5%	1–40%	0–3%	2–42%
	2	0.2	60–80	1–7%	1–8%	1–12%	0–3%	1–15%

are a property of the inclusively-measured jet population and are thus typically normalized as such in theoretical calculations [17].

The ungroomed jet angularity distributions are shown in Fig. 1 and Fig. 2 for $R = 0.4$ and $R = 0.2$, respectively. By the definitions given in Eq. 2, these distributions are all normalized to unity. As α increases, the distributions skew towards small λ_α , since θ_i is smaller than unity. For larger R , the distributions are narrower than for smaller R , as expected due to the collinear nature of jet fragmentation. For small R and low $p_T^{\text{ch jet}}$ there is a visible peak at $\lambda_\alpha = 0$, which is due to single particle jets. These distributions are compared to PYTHIA8 Monash 2013 [49, 66] and Herwig7 (default tune) [50, 51] from truth-level projections of the respective response matrices, with jet reconstruction assigning tracks the π^\pm meson mass as in the measured data. These comparisons show deviations up to approximately +50% (–30%). The largest deviations are for small values of λ_α , where nonperturbative physics becomes significant (see Sec. 5.1 for discussion).

The groomed jet angularity distributions for $z_{\text{cut}} = 0.2$ and $\beta = 0$ are shown in Fig. 3 for $R = 0.4$ and Fig. 4 for $R = 0.2$. Note that these distributions are shown on a logarithmic scale due to the distributions being more strongly peaked and falling faster with λ_α as compared to the ungroomed distributions. The groomed jet angularities have significantly smaller values than the ungroomed jet angularities, due to the removal of soft wide-angle radiation. The fraction of “untagged” jets, those that do not contain a splitting which passes the Soft Drop condition, ranges from 10 to 12%. Unlike the ungroomed jet angularities, which are normalized to unity, the groomed jet angularities are normalized to the Soft Drop tagging fraction. Since the tagging rate is fairly large, the measured distributions are therefore normalized close to unity. PYTHIA and Herwig describe the groomed jet angularities slightly better than the ungroomed jet angularities, with most deviations seen in the ungroomed distributions improving by 10–20% in the groomed case. Comparing to the two MC generators, the data are in slightly better agreement with Herwig7 than with PYTHIA8, especially for $R = 0.4$.

The data cover a wide range of α and multiple R down to low p_T , and therefore are subject to varying influence from nonperturbative effects. Accordingly, these data can be used to study nonperturbative effects. The level and location of the disagreements with PYTHIA and Herwig provide further constraints on nonperturbative effects in MC event generators. Moreover, the comparison of the groomed

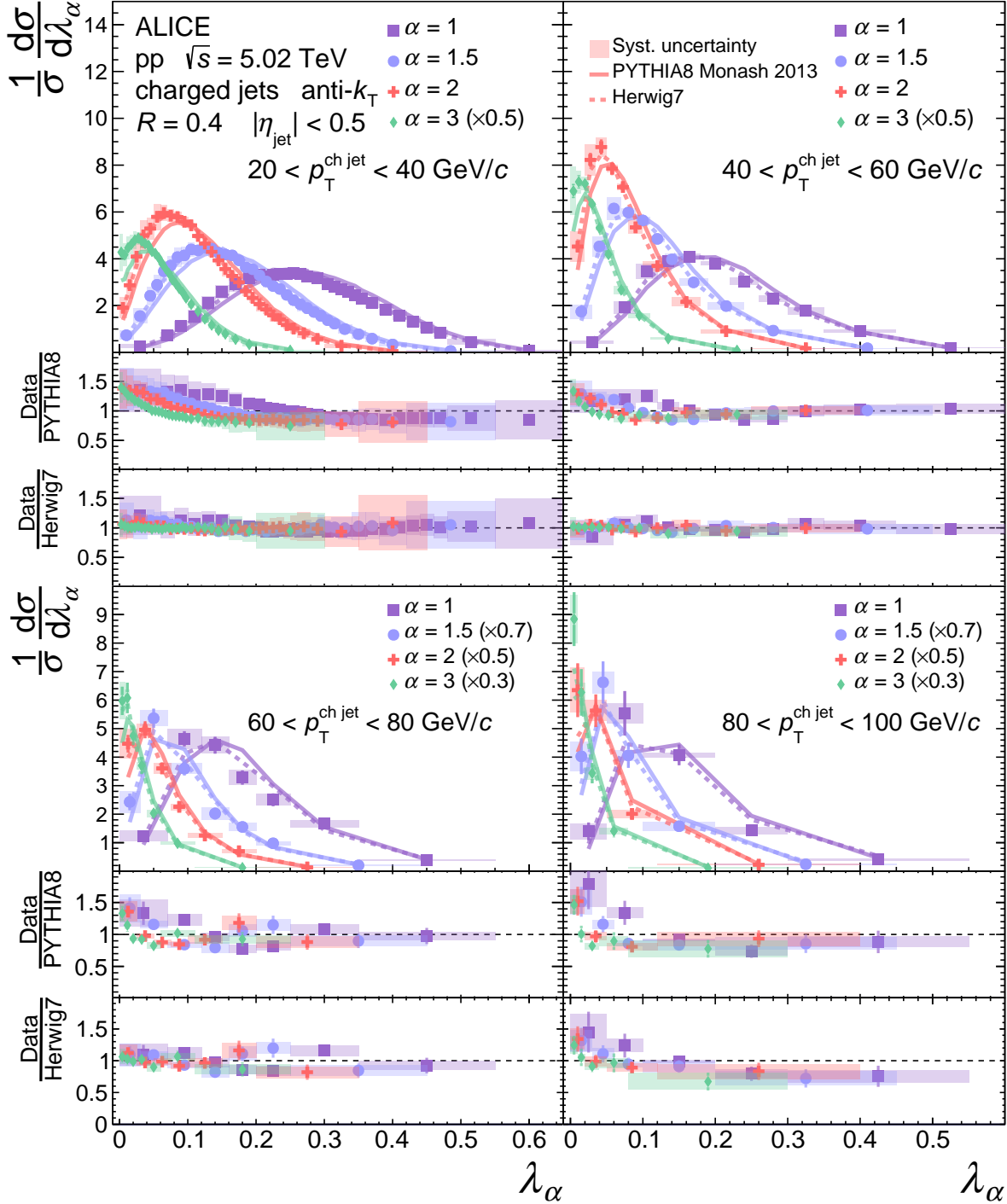


Figure 1: Comparison of ungroomed jet angularities λ_α in pp collisions for $R = 0.4$ to MC predictions using PYTHIA8 and Herwig7, as described in the text. Four equally-sized $p_T^{\text{ch jet}}$ intervals are shown, with edges ranging between 20 and 100 GeV/c. The distributions are normalized to unity.

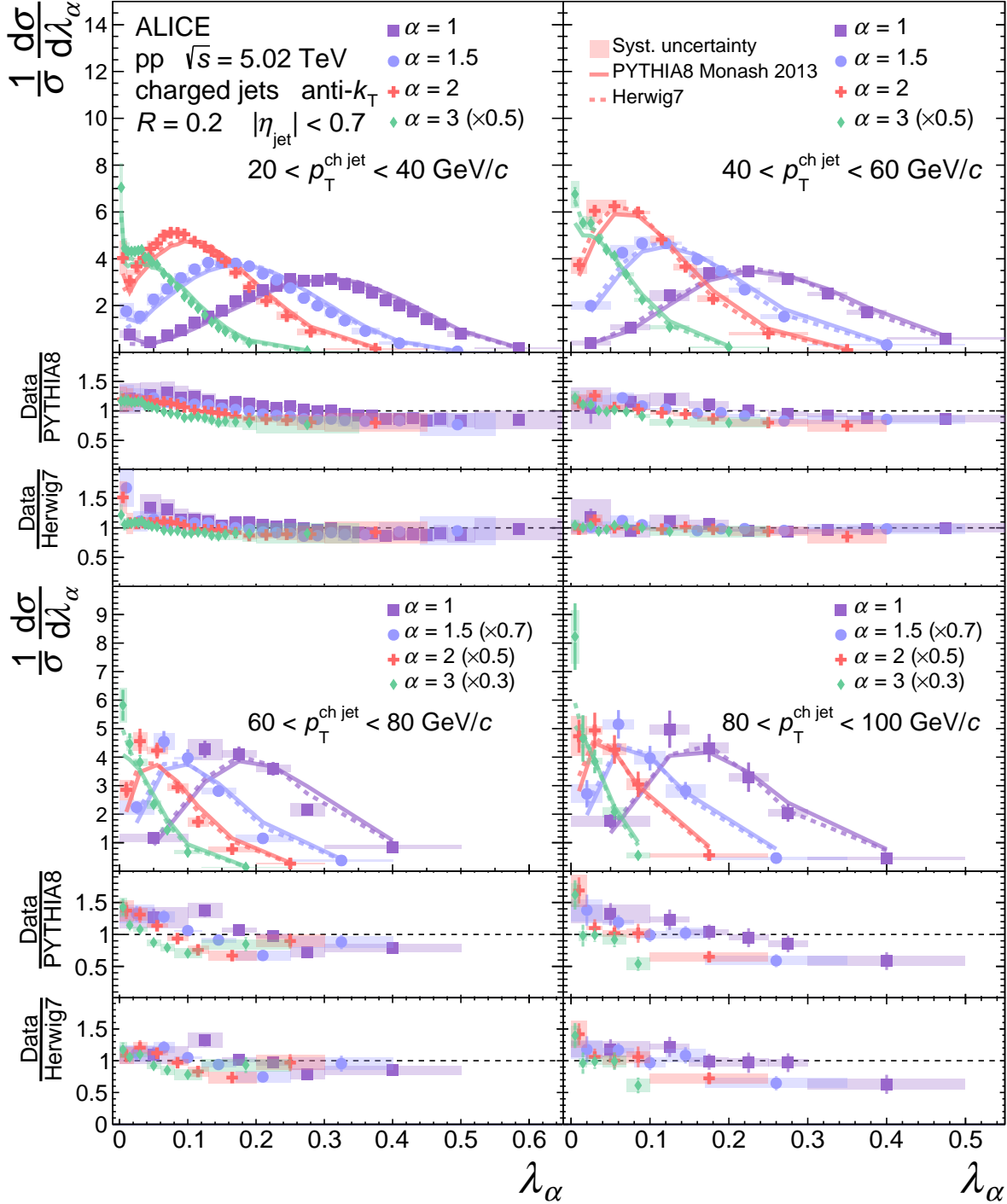


Figure 2: Comparison of ungroomed jet angularities λ_α in pp collisions for $R = 0.2$ to MC predictions using PYTHIA8 and Herwig7, as described in the text. Four equally-sized $p_T^{\text{ch jet}}$ intervals are shown, with edges ranging between 20 and 100 GeV/c. The distributions are normalized to unity.

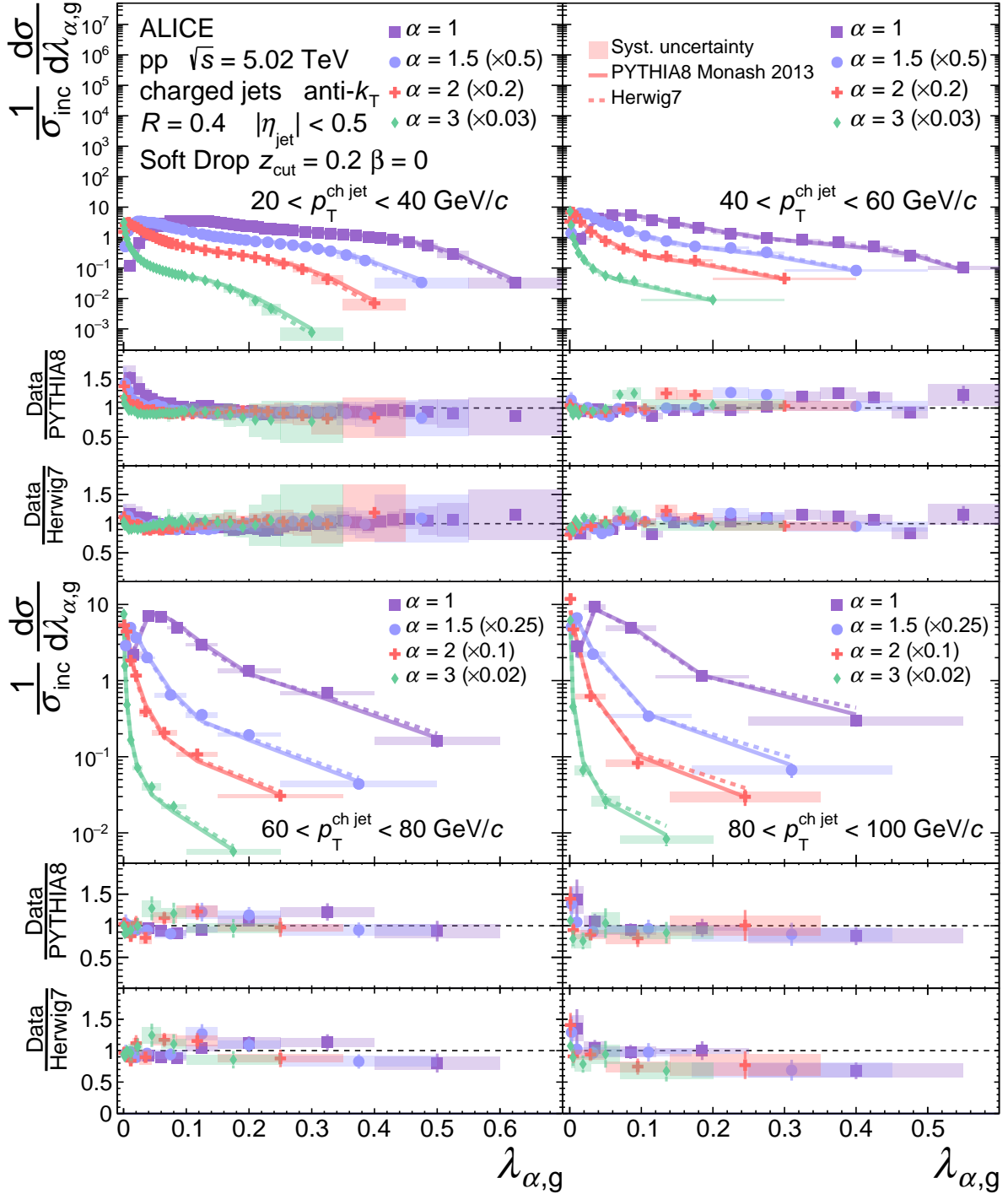


Figure 3: Comparison of groomed jet angularities $\lambda_{\alpha,g}$ in pp collisions for $R = 0.4$ to MC predictions using PYTHIA8 and Herwig7, as described in the text. Four equally-sized $p_T^{\text{ch jet}}$ intervals are shown between 20 and 100 GeV/c. The distributions are normalized to the groomed jet tagging fraction.

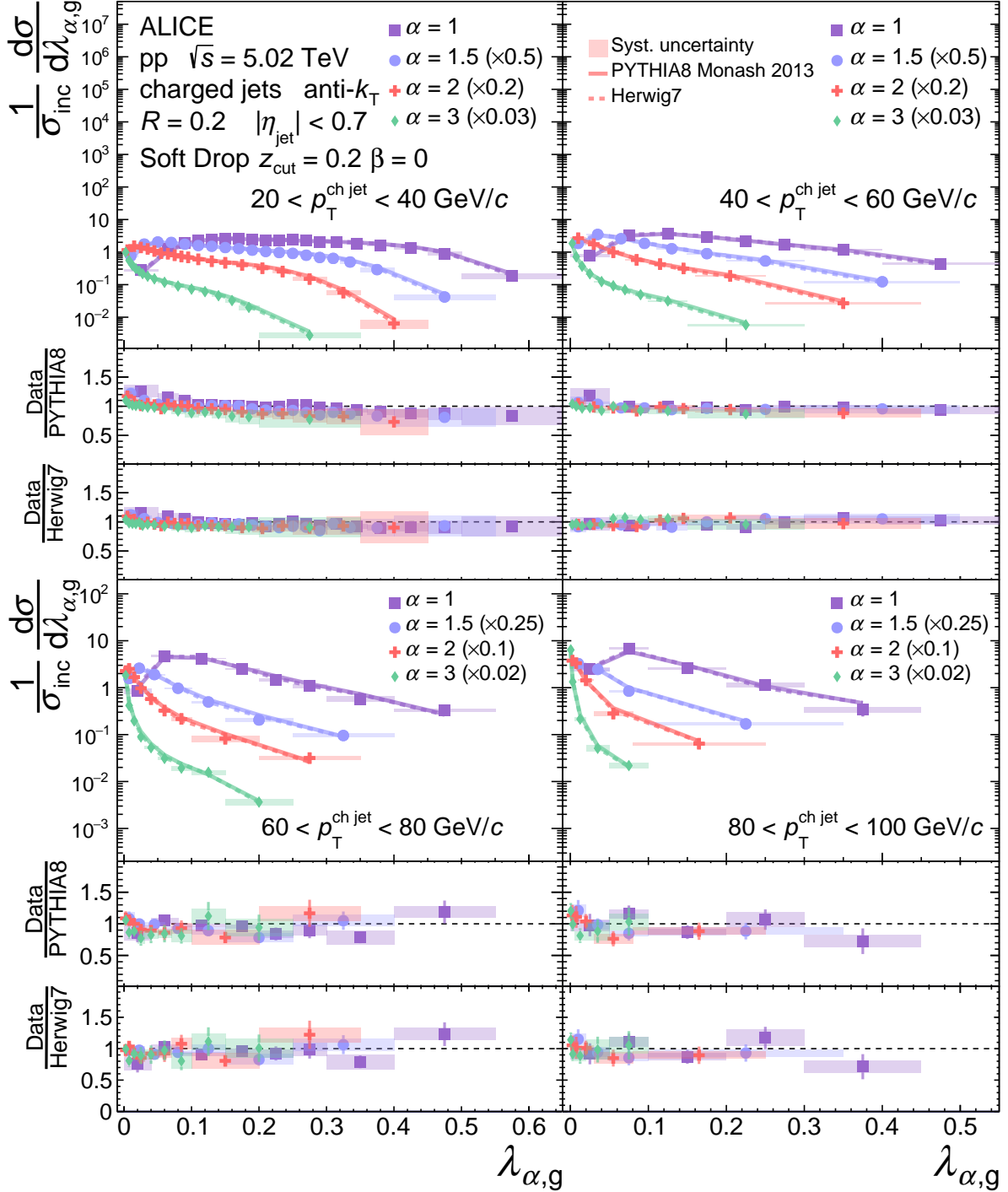


Figure 4: Comparison of groomed jet angularities $\lambda_{\alpha,g}$ in pp collisions for $R = 0.2$ to MC predictions using PYTHIA8 and Herwig7, as described in the text. Four equally-sized $p_T^{\text{ch jet}}$ intervals are shown between 20 and 100 GeV/c. The distributions are normalized to the groomed jet tagging fraction.

and the ungroomed jet angularities with MC event generators allows direct sensitivity to radiation that was groomed away, which is highly nonperturbative.

5.1 Comparison to analytical calculations

The measured ungroomed and groomed jet angularities are compared with analytical calculations [9, 17] which use all-order resummations of large logarithms to next-to-leading logarithmic (NLL') accuracy [19]. In particular, the calculations resum logarithms of λ_α , R , and z_{cut} . In the case of the λ_α logarithms, the cumulant of the cross section includes the complete set of terms of form $\alpha_s^n \ln^k \lambda_\alpha$ for $k = 2n, 2n - 1$, and $2n - 2$. The calculations are valid up to power corrections in λ_α , R , and z_{cut} , and do not include non-global logarithms [72]. These calculations are based on the framework of Soft Collinear Effective Theory (SCET) [73], in which the jet cross section is factorized into a ‘‘hard function’’ corresponding to the initial scattering, and a ‘‘jet function’’ corresponding to the fragmentation of a hard-scattered parton into a jet. For the calculation of the jet angularities, the jet function is then further factorized into collinear and soft functions. Systematic uncertainties on the analytical predictions are estimated by systematically varying fifteen combinations of scales that emerge in the calculation.

For the ungroomed jet angularities, the collinear-soft momentum scale for the factorization formalism becomes nonperturbative for [9]

$$\lambda_\alpha \lesssim \frac{\Lambda}{p_{\text{T}}^{\text{ch jet}} R}, \quad (3)$$

where Λ is the energy scale at which α_s becomes nonperturbative, which is taken to be approximately 1 GeV/ c . For the groomed jet angularities with $\beta = 0$, this soft factorization scale becomes nonperturbative for [17]

$$\lambda_{\alpha,\text{g}} \lesssim z_{\text{cut}}^{1-\alpha} \left(\frac{\Lambda}{p_{\text{T}}^{\text{ch jet}} R} \right)^\alpha. \quad (4)$$

Accordingly, the analytical predictions are expected to describe the data only at sufficiently large λ_α , which depends on $p_{\text{T}}^{\text{ch jet}}$, R , and z_{cut} . On the other hand, for $\lambda_\alpha = \mathcal{O}(1)$, power corrections in λ_α become important, and are not included in the NLL' calculations. Note that for $\lambda_{\alpha,\text{g}} > z_{\text{cut}}$, the groomed and ungroomed predictions are identical at the parton level.

For values of λ_α that are sufficiently large to be described by SCET, corrections for nonperturbative effects must still be applied in order to compare these parton-level calculations to our charged-hadron-level measurements. These nonperturbative effects include hadronization, the underlying event, and the selection of charged particle jets. Note that track-based observables are IRC-unsafe. In general, nonperturbative track functions can be used to directly compare track-based measurements to analytical calculations [16, 74, 75]; however, such an approach has not yet been developed for jet angularities. Two techniques are used, described in the following subsections, to apply the nonperturbative corrections.

5.1.1 MC-based hadronization correction

The first technique relies solely on MC generators to transform the parton-level calculations into the final predictions at the charged-hadron level. Two response matrices are constructed, one using PYTHIA 8.244 and the other using Herwig7, which map the jet angularity distributions from jets reconstructed at the final-state parton level (after the parton shower) to those from jets reconstructed at the charged-hadron level. This is done by requiring a unique geometrical match between the parton and charged-hadron-level jets of $\Delta R < R/2$. The PYTHIA8 simulation uses the default Monash 2013 tune, which is tuned to both e^+e^- and $p\bar{p}$ data [66], with the only change being that the minimum shower p_{T} (TimeShower:pTmin) is set to 0.2 GeV/ c , one half of its default value, in order to better match the NLL' predictions at parton level. Herwig7 is also run with the default tune [76]. The response matrix generated with both MC simulations is 4D, mapping $p_{\text{T}}^{\text{parton jet}}$ and $\lambda_\beta^{\text{parton jet}}$ to $p_{\text{T},\text{truth}}^{\text{ch jet}}$ and $\lambda_{\alpha,\text{truth}}$.

Since the NLL' predictions are generated as normalized distributions, each $p_T^{\text{ch jet}}$ interval is first scaled by a value corresponding to the inclusive p_T^{jet} cross section, calculated at Next-to-Leading Order (NLO) with NLL resummation of logarithms in the jet radius [77]. The 4D response matrix discussed above is then multiplied by these scaled 2D NLL' predictions (in both p_T^{jet} , ranging from 10 to 200 GeV/c, and λ_α) to obtain the theoretical predictions at charged-hadron level. To propagate the systematic uncertainty on the original NLL' calculations, this ‘‘folding’’ procedure is performed individually for each of fifteen scale variations, from which a total systematic uncertainty is constructed from the minimum and maximum variation in each interval. Note that this procedure introduces a model-dependence to the comparison, and in fact significantly reduces the magnitude of the systematic uncertainties compared to the parton level; the repetition of this procedure with both PYTHIA8 and Herwig7 is meant to estimate the size of this model dependence.

Although the perturbative accuracy of the MC generators is not clear, by restricting these comparisons to $p_T^{\text{ch jet}} > 60$ GeV/c, there is adequate matching between the analytical calculations and the MC generators' final-state parton-level predictions to employ the nonperturbative corrections via this mapping procedure. After the folding step, an additional bin-by-bin correction is applied for multi-parton interactions in the underlying event using the respective event generator. More specifically, a ratio is created between the 2D jet angularity distributions generated with multi-parton interactions on versus off at the charged-hadron level, which is then multiplied bin-by-bin by the folded distributions. In all cases, the corrections performed with PYTHIA and those with Herwig are similar in magnitude, indicating that this correction procedure is reasonable.

Figure 5 shows comparisons of the measured ungroomed jet angularities to the folded theoretical predictions for $60 < p_T^{\text{ch jet}} < 80$ GeV/c, for both $R = 0.2$ (top) and $R = 0.4$ (bottom) and for $\alpha = 1.5$ (left), 2 (middle), and 3 (right). Figure 6 shows the corresponding comparisons for the groomed jet angularities. The comparisons for $80 < p_T^{\text{ch jet}} < 100$ GeV/c are shown in Appendix A. Predictions for the $\alpha = 1$ distributions are not currently available due to enhanced sensitivity to soft-recoil, which requires a different factorization [22].

A dashed vertical line is drawn as a rough estimate for the division of perturbative- and nonperturbative-dominated regions, via Eq. 3 or Eq. 4 with $\Lambda = 1$ GeV/c and the mean $p_T^{\text{ch jet}}$ for each interval. Note that the transition from values of λ_α which are dominated by perturbative versus nonperturbative physics is actually smooth, and this vertical line is merely intended as a visual guide. The nonperturbative-dominated region of the jet angularities is denoted as $\lambda_\alpha^{\text{NP}}$.

Since the integral for all of the distributions in Fig. 1 through Fig. 4 is fixed at unity by construction, it is important to note that disagreement in the nonperturbative-dominated region induces disagreement in the perturbative-dominated region. Discrepancy in the nonperturbative region is expected due to the divergence of α_s and the corresponding significance of higher-order terms in the perturbative expansion — and will necessarily induce disagreement in the perturbative-dominated region. Accordingly, for these theoretical comparisons, the distributions are normalized such that the integral above $\lambda_\alpha^{\text{NP}}$ is unity.

5.1.2 Shape function based correction

An alternate correction technique is also used, which employs a nonperturbative shape function $F(k)$ [14, 20, 21] to correct for the effects caused by hadronization and the underlying event. The shape function is defined as

$$F(k) = \frac{4k}{\Omega_\alpha^2} \exp\left(-\frac{2k}{\Omega_\alpha}\right), \quad (5)$$

where k is a momentum scale parameter of the shape function, and Ω_α is described by a single parameter $\Omega = \mathcal{O}(1 \text{ GeV}/c)$ obeying the scaling relation

$$\Omega_\alpha = \Omega/(\alpha - 1), \quad (6)$$

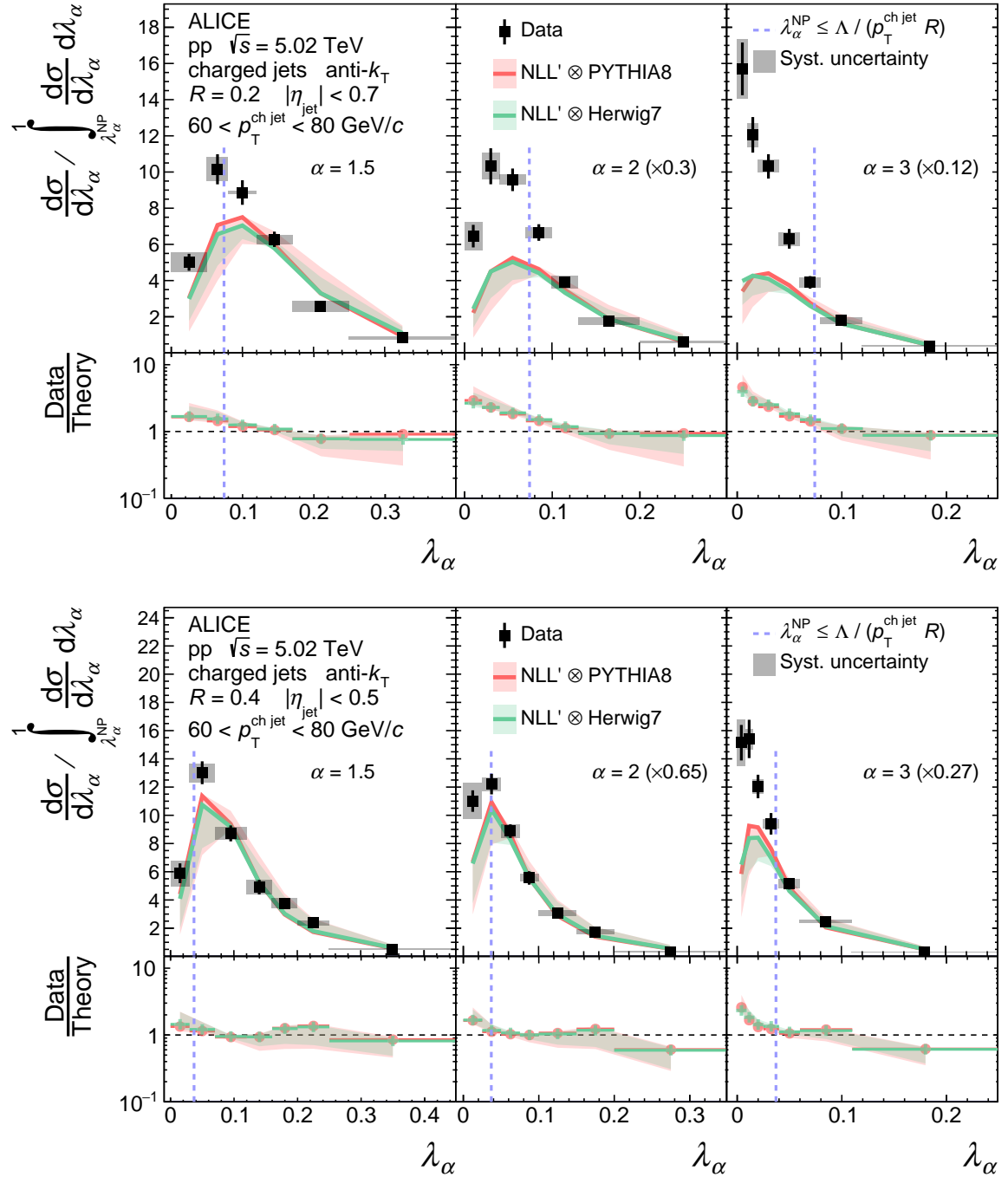


Figure 5: Comparison of ungroomed jet angularities λ_α in pp collisions for $R = 0.2$ (top) and $R = 0.4$ (bottom) to analytical NLL' predictions with MC hadronization corrections in the range $60 < p_T^{\text{ch jet}} < 80$ GeV/c. The distributions are normalized such that the integral of the perturbative region defined by $\lambda_\alpha > \lambda_\alpha^{\text{NP}}$ (to the right of the dashed vertical line) is unity. Divided bins are placed into the left (NP) region.

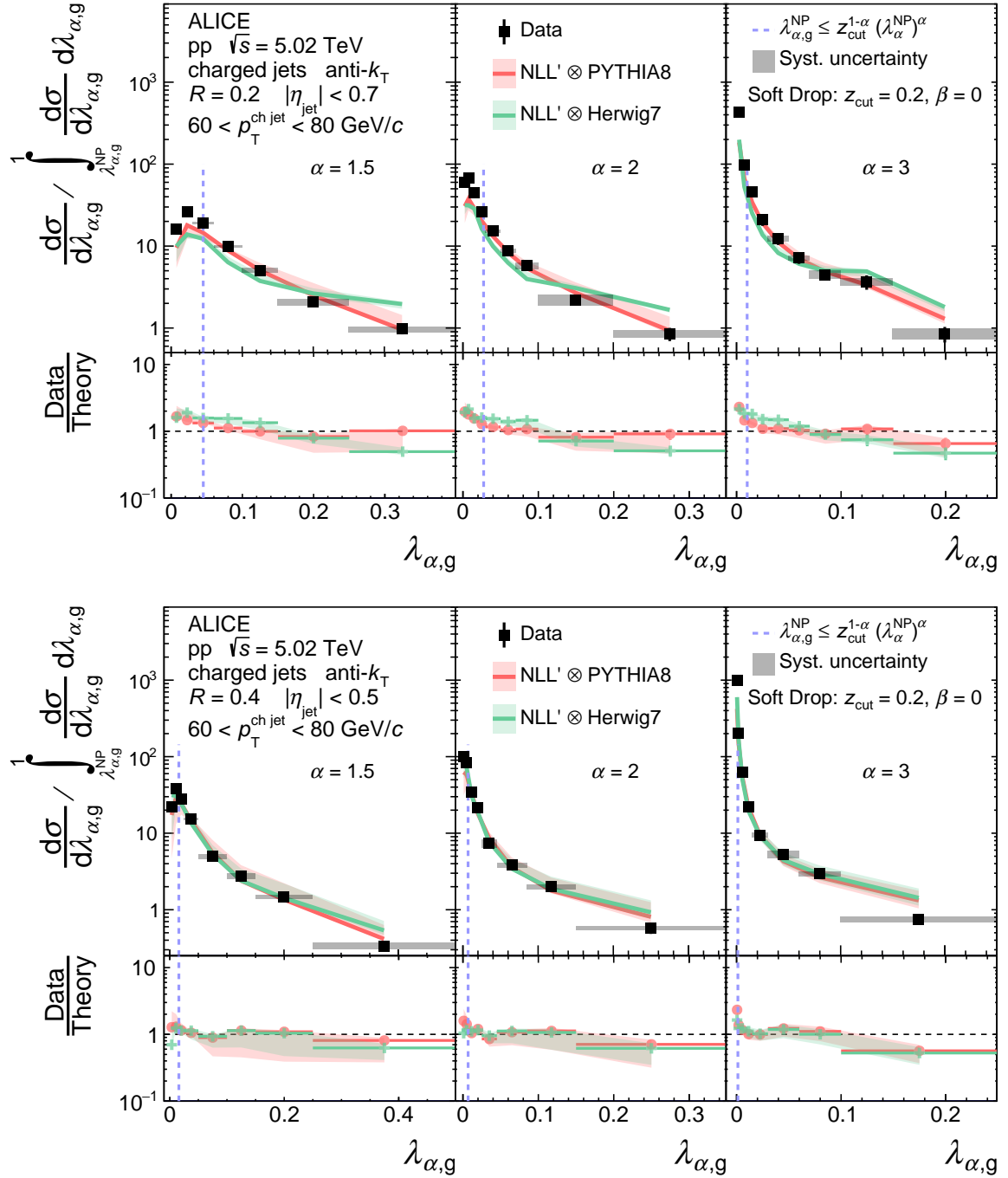


Figure 6: Comparison of groomed jet angularities $\lambda_{\alpha,g}$ in pp collisions for $R = 0.2$ (top) and $R = 0.4$ (bottom) to analytical NLL' predictions with MC hadronization corrections in the range $60 < p_T^{\text{ch jet}} < 80$ GeV/c. The distributions are normalized such that the integral of the perturbative region defined by $\lambda_{\alpha,g} > \lambda_{\alpha,g}^{\text{NP}}$ (to the right of the dashed vertical line) is unity. Divided bins are placed into the left (NP) region.

and expected to hold universally for hadronization corrections (but not necessarily for underlying event corrections). To correct the parton-level calculations to the hadron level, this shape function is convolved with the perturbative (parton level) jet angularity distribution via numerical integration over argument k

$$\frac{d\sigma}{dp_T^{\text{jet}} d\lambda_\alpha} = \int F(k) \frac{d\sigma_{\text{pert}}}{dp_T^{\text{jet}} d\lambda_\alpha} \left(\lambda_\alpha - \lambda_\alpha^{\text{shift}}(k) \right) dk, \quad (7)$$

where the shift term $\lambda_\alpha^{\text{shift}}(k)$ is either [17, 21]:

$$\lambda_\alpha^{\text{shift}}(k) = \frac{k}{p_T^{\text{jet}} R} \text{ (ungroomed), or } z_{\text{cut}}^{1-\alpha} \left(\frac{k}{p_T^{\text{jet}} R} \right)^\alpha \text{ (groomed, with } \beta = 0). \quad (8)$$

The limits of the integral are thus given by the values of k for which the argument $(\lambda_\alpha - \lambda_\alpha^{\text{shift}}(k))$ is between 0 and 1. Since the nonperturbative parameter Ω is not calculable within perturbation theory, four values (0.2, 0.4, 0.8, and 2 GeV/ c) are chosen to observe the different shifting effects. These distributions are then corrected once more using a similar PYTHIA8 folding procedure as described above to account for the effects of only reconstructing charged-particle jets. This correction is dominated by a shift and smearing along the p_T^{jet} axis.

The comparisons to the ungroomed predictions are shown in Fig. 7, and the groomed predictions are shown in Fig. 8. The shape function approach, specifically the scaling given in Eq. 6, is not fully justified in the groomed case [78, 79]; nevertheless, reasonable agreement is observed. Since this shape convolution does not require matching to MC at the parton level, the comparisons are extended to the $40 < p_T^{\text{ch jet}} < 60$ GeV/ c interval, but below this the perturbative accuracy of the parton-level predictions is insufficient for rigorous comparisons. The comparisons for $40 < p_T^{\text{ch jet}} < 60$ GeV/ c and $80 < p_T^{\text{ch jet}} < 100$ GeV/ c are shown in Appendix A.

5.2 Discussion

The λ_α distributions are generally consistent with the calculations within uncertainties when λ_α is sufficiently large to be in the pQCD regime. This holds approximately independent of α , R , and p_T^{jet} , and whether or not the jets are groomed. In some distributions, however, particularly for $R = 0.4$, modest disagreement is observed at large λ_α . This disagreement cannot be unambiguously associated with a particular value of λ_α due to the self-normalization of the observable, but rather demonstrates an overall inconsistency in the shape of the distribution. This disagreement could be caused by the unaccounted power corrections in λ_α , or other effects — and suggests a need for further theoretical investigation. Nevertheless, the overall agreement with the perturbative calculations is striking, given the low-to-moderate jet p_T and R considered.

For $\alpha = 1.5$, the majority of the distributions can be described perturbatively, as $\lambda_\alpha^{\text{NP}}$ is confined towards the left-hand side of the distributions. As α increases to $\alpha = 3$, the influence of the $\lambda_\alpha^{\text{NP}}$ region grows, and the ungroomed distributions become strongly nonperturbative. Similarly, as R increases from $R = 0.2$ to $R = 0.4$, or as $p_T^{\text{ch jet}}$ increases, the size of the perturbative region increases. In the nonperturbative region $\lambda_\alpha < \lambda_\alpha^{\text{NP}}$, the λ_α distributions diverge from the calculations. This is expected, since the perturbative approximations break down for $\lambda_\alpha < \lambda_\alpha^{\text{NP}}$, and neither the MC or shape function corrections are necessarily expected to fully correct for missing physics at higher orders or for nonperturbative coupling. In some distributions, the shape-function-based correction is sometimes able to describe the data partially into the nonperturbative regime for suitable values of Ω .

While the overall level of agreement is comparable in both the ungroomed and groomed cases, grooming widens the pQCD regime, as indicated by the location of the dashed blue line in Figures [5-8]. On the other hand, grooming shifts the distributions themselves to significantly smaller values of λ_α . Nevertheless, this highlights the potential benefit of grooming in heavy-ion collisions in order to retain a larger degree of perturbative control in addition to controlling effects of the underlying event.

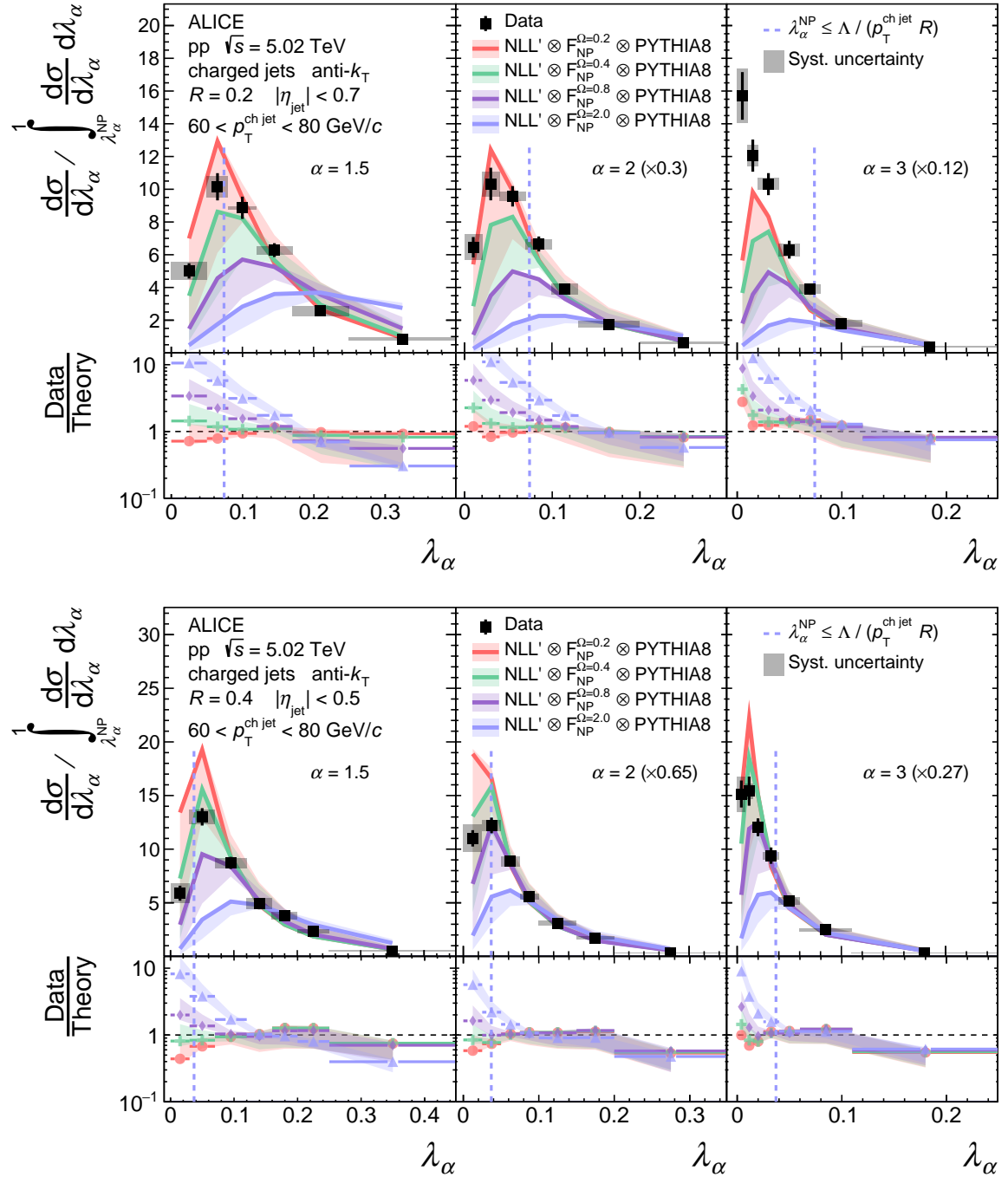


Figure 7: Comparison of ungroomed jet angularities λ_{α} in pp collisions for $R = 0.2$ (top) and $R = 0.4$ (bottom) to analytical NLL' predictions using $F(k)$ convolution in the range $60 < p_T^{\text{ch,jet}} < 80$ GeV/c. The distributions are normalized such that the integral of the perturbative region defined by $\lambda_{\alpha} > \lambda_{\alpha}^{\text{NP}}$ (to the right of the dashed vertical line) is unity. Divided bins are placed into the left (NP) region.

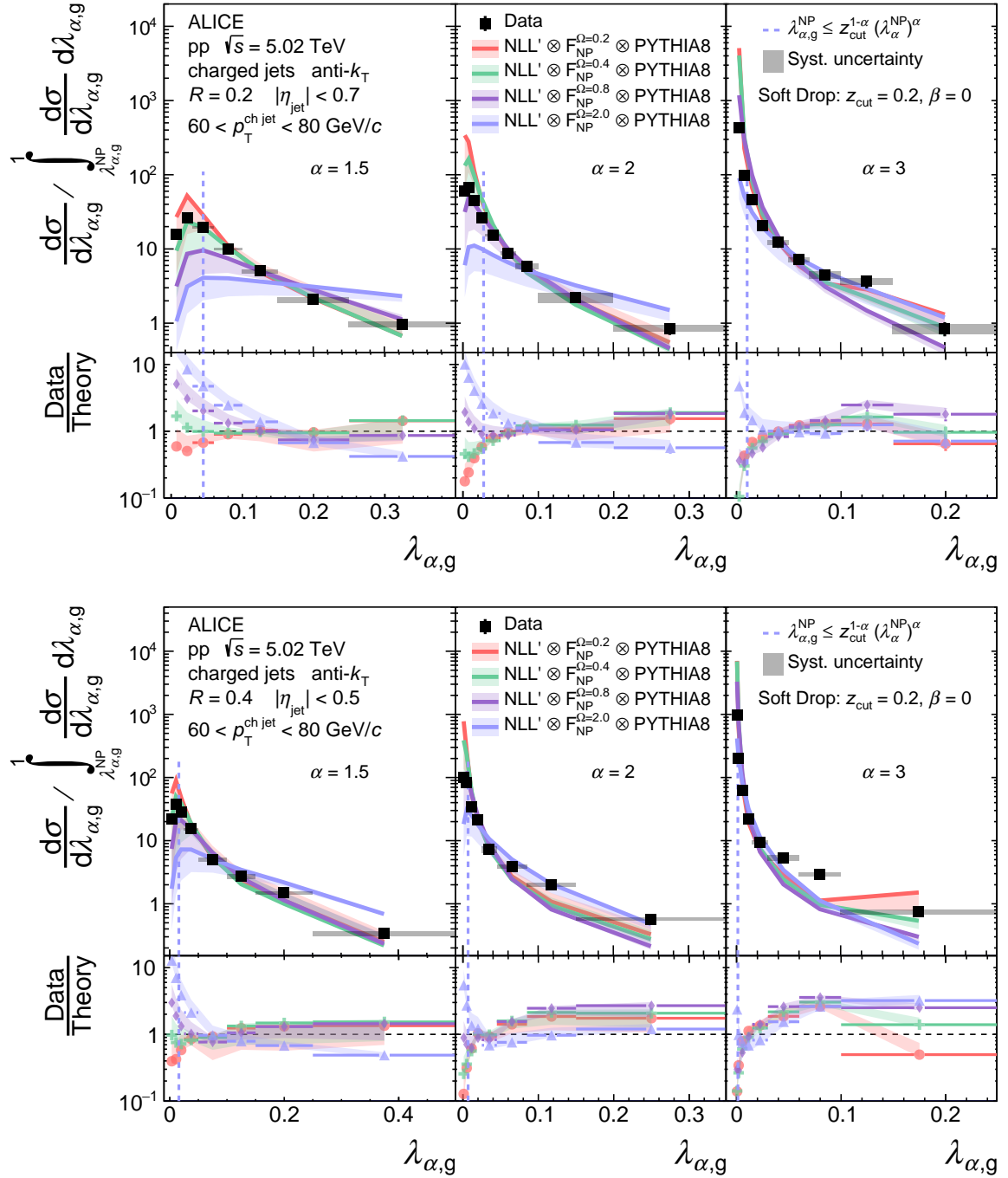


Figure 8: Comparison of groomed jet angularities $\lambda_{\alpha,g}$ in pp collisions for $R = 0.2$ (top) and $R = 0.4$ (bottom) to analytical NLL' predictions using $F(k)$ convolution in the range $60 < p_T^{\text{ch,jet}} < 80$ GeV/c. The distributions are normalized such that the integral of the perturbative region defined by $\lambda_{\alpha,g} > \lambda_{\alpha,g}^{\text{NP}}$ (to the right of the dashed vertical line) is unity. Divided bins are placed into the left (NP) region.

The performance of the two nonperturbative correction methods — based entirely on MC generators, or on shape functions — are comparable in the perturbative regime. Comparing different values of Ω for the ungroomed case, where Eq. 6 is justified, there is in many cases only a small difference between the calculations with $\Omega = 0.2, 0.4,$ and 0.8 GeV/ c . However, for $\alpha = 1.5$ and $\alpha = 2$, larger values of Ω ($\Omega = 2$ GeV/ c) appear to have more tension with the data in the perturbative regime than smaller values. For $\alpha = 3$, the perturbative region is too small to make any clear statement. One must bear in mind, however, that $\lambda_{\alpha}^{\text{NP}}$ is only a rough characterization of the regime of validity of the perturbative calculation. Consequently, it is unknown whether this disagreement is due to the value of Ω or due to the breakdown of the perturbative calculation. For smaller values of Ω (e.g. $\Omega = 0.2$ or 0.4 GeV/ c), the predicted scaling of Eq. 6 is consistent with the data. Note that the value of Ω which describes the data is $\mathcal{O}(1)$ as expected for hadronization corrections. These smaller values contrast with a previous result of $\Omega = 3.5$ GeV/ c for the ungroomed mass of $R = 0.4$ jets at $200 < p_{\text{T}}^{\text{jet}} < 300$ GeV/ c [80], suggesting that the underlying event contribution to Ω , which is not expected to obey the scaling of Eq. 6, may be modified by jets measured at different $p_{\text{T}}^{\text{jet}}$ or by the choice to reconstruct jets using only charged-particle tracks. No significant R -dependence is observed in the scaling behavior in this analysis, suggesting that any scaling-breaking underlying event contributions, when also combined with hadronization corrections, are small for $R = 0.2$ and 0.4 .

6 Conclusion

The generalized jet angularities are reported both with and without Soft Drop grooming, $\lambda_{\alpha,\text{g}}$ and λ_{α} , respectively, for charged-particle jets in pp collisions at $\sqrt{s} = 5.02$ TeV with the ALICE detector. This measurement of both the ungroomed and, for the first time, the groomed jet angularities provides constraints on models and captures the interplay between perturbative and nonperturbative effects in QCD. Systematic variations of the contributions from collinear and soft radiation of the shower, captured within a given R , are provided by measuring the jet angularities for a selection of α parameters. These results consequently provide rigorous tests of pQCD calculations.

The theoretical predictions at NLL' in SCET show an overall agreement with the data for jets with values of λ_{α} in the perturbative regime delimited by a collinear-soft momentum scale in the factorization framework of about 1 GeV/ c . The calculations, after accounting for nonperturbative effects by two different methods, are compatible within about 20% or better with the data in the perturbative region for all explored values of R and α . However, larger deviations of up to about 50% are observed in the tails of some distributions, suggesting a need for further theoretical study. By making comparisons solely in the perturbatively-dominated regime, consistency is seen with a predicted universal scaling of the nonperturbative shape function parameter Ω_{α} with value $\Omega < 1$. A clear breakdown of the agreement is observed for small λ , where the perturbative calculation is expected to fail. Such nonperturbative effects include soft splittings and hadronization, and these effects dominate over significant regions of the phase space of moderate and low-energy jets. This is corroborated by the comparison of the measured groomed jet angularities to the equivalent theoretical calculations, which demonstrate a wider range of agreement with the perturbative calculations.

These comparisons provide critical guidance for measurements in high-energy heavy-ion collisions where the internal structure of jets may undergo modifications via scatterings of jet fragments with the hot and dense QCD medium. Our measurements demonstrate that any comparison to pQCD must also consider the regimes of λ_{α} and $\lambda_{\alpha,\text{g}}$ that are controlled by perturbative processes as opposed to those that are dominated by nonperturbative processes. This provides guidance for the selections of α , R , and $p_{\text{T}}^{\text{ch jet}}$, and indicates the importance of capturing the complete spectrum of processes (perturbative and non-perturbative) in theory calculations attempting to explain jet quenching.

These measurements further highlight that disagreement between theoretical predictions and data in the

nonperturbative regime will necessarily induce disagreement in the perturbative regime, when in fact the perturbative accuracy of predictions should only be scrutinized within the perturbative regime. In practice, these measurements give a clear indication that careful inspection is needed when interpreting measurements of jet substructure based on models of jet quenching in heavy-ion collisions for observables including the jet angularity and the jet mass. Future measurements will benefit from the provided guidance demonstrating not only the agreement of jet angularities with pQCD calculations in the perturbative regime but also on selecting on jet angularity differentially with α , R , and $p_T^{\text{ch jet}}$ in order to maximize theoretical control and interpretation of the perturbative and nonperturbative regimes of jet substructure observables.

Acknowledgements

We gratefully acknowledge Kyle Lee and Felix Ringer for providing theoretical predictions, and for valuable discussions regarding the comparison of these predictions to our measurements.

The ALICE Collaboration would like to thank all its engineers and technicians for their invaluable contributions to the construction of the experiment and the CERN accelerator teams for the outstanding performance of the LHC complex. The ALICE Collaboration gratefully acknowledges the resources and support provided by all Grid centres and the Worldwide LHC Computing Grid (WLCG) collaboration. The ALICE Collaboration acknowledges the following funding agencies for their support in building and running the ALICE detector: A. I. Alikhanyan National Science Laboratory (Yerevan Physics Institute) Foundation (ANSL), State Committee of Science and World Federation of Scientists (WFS), Armenia; Austrian Academy of Sciences, Austrian Science Fund (FWF): [M 2467-N36] and Nationalstiftung für Forschung, Technologie und Entwicklung, Austria; Ministry of Communications and High Technologies, National Nuclear Research Center, Azerbaijan; Conselho Nacional de Desenvolvimento Científico e Tecnológico (CNPq), Financiadora de Estudos e Projetos (Finep), Fundação de Amparo à Pesquisa do Estado de São Paulo (FAPESP) and Universidade Federal do Rio Grande do Sul (UFRGS), Brazil; Ministry of Education of China (MOEC), Ministry of Science & Technology of China (MSTC) and National Natural Science Foundation of China (NSFC), China; Ministry of Science and Education and Croatian Science Foundation, Croatia; Centro de Aplicaciones Tecnológicas y Desarrollo Nuclear (CEADEN), Cubaenergía, Cuba; Ministry of Education, Youth and Sports of the Czech Republic, Czech Republic; The Danish Council for Independent Research | Natural Sciences, the VILLUM FONDEN and Danish National Research Foundation (DNRF), Denmark; Helsinki Institute of Physics (HIP), Finland; Commissariat à l’Energie Atomique (CEA) and Institut National de Physique Nucléaire et de Physique des Particules (IN2P3) and Centre National de la Recherche Scientifique (CNRS), France; Bundesministerium für Bildung und Forschung (BMBF) and GSI Helmholtzzentrum für Schwerionenforschung GmbH, Germany; General Secretariat for Research and Technology, Ministry of Education, Research and Religions, Greece; National Research, Development and Innovation Office, Hungary; Department of Atomic Energy Government of India (DAE), Department of Science and Technology, Government of India (DST), University Grants Commission, Government of India (UGC) and Council of Scientific and Industrial Research (CSIR), India; Indonesian Institute of Science, Indonesia; Istituto Nazionale di Fisica Nucleare (INFN), Italy; Institute for Innovative Science and Technology, Nagasaki Institute of Applied Science (IIST), Japanese Ministry of Education, Culture, Sports, Science and Technology (MEXT) and Japan Society for the Promotion of Science (JSPS) KAKENHI, Japan; Consejo Nacional de Ciencia (CONACYT) y Tecnología, through Fondo de Cooperación Internacional en Ciencia y Tecnología (FONCICYT) and Dirección General de Asuntos del Personal Académico (DGAPA), Mexico; Nederlandse Organisatie voor Wetenschappelijk Onderzoek (NWO), Netherlands; The Research Council of Norway, Norway; Commission on Science and Technology for Sustainable Development in the South (COMSATS), Pakistan; Pontificia Universidad Católica del Perú, Peru; Ministry of Education and Science, National Science Centre and WUT ID-UB, Poland; Korea Institute of Science and Technol-

ogy Information and National Research Foundation of Korea (NRF), Republic of Korea; Ministry of Education and Scientific Research, Institute of Atomic Physics and Ministry of Research and Innovation and Institute of Atomic Physics, Romania; Joint Institute for Nuclear Research (JINR), Ministry of Education and Science of the Russian Federation, National Research Centre Kurchatov Institute, Russian Science Foundation and Russian Foundation for Basic Research, Russia; Ministry of Education, Science, Research and Sport of the Slovak Republic, Slovakia; National Research Foundation of South Africa, South Africa; Swedish Research Council (VR) and Knut & Alice Wallenberg Foundation (KAW), Sweden; European Organization for Nuclear Research, Switzerland; Suranaree University of Technology (SUT), National Science and Technology Development Agency (NSDTA) and Office of the Higher Education Commission under NRU project of Thailand, Thailand; Turkish Energy, Nuclear and Mineral Research Agency (TENMAK), Turkey; National Academy of Sciences of Ukraine, Ukraine; Science and Technology Facilities Council (STFC), United Kingdom; National Science Foundation of the United States of America (NSF) and United States Department of Energy, Office of Nuclear Physics (DOE NP), United States of America.

References

- [1] R. Kogler *et al.*, “Jet substructure at the Large Hadron Collider”, *Rev. Mod. Phys.* **91** (Dec, 2019) 045003, arXiv:1803.06991 [hep-ex].
- [2] A. J. Larkoski, I. Moulton, and B. Nachman, “Jet substructure at the Large Hadron Collider: A review of recent advances in theory and machine learning”, *Phys. Rept.* **841** (Jan, 2020) 1–63, arXiv:1709.04464 [hep-ph].
- [3] A. J. Larkoski, S. Marzani, G. Soyez, and J. Thaler, “Soft Drop”, *JHEP* **05** (May, 2014) 146, arXiv:1402.2657 [hep-ph].
- [4] M. Dasgupta, A. Fregoso, S. Marzani, and G. P. Salam, “Towards an understanding of jet substructure”, *JHEP* **09** (Sep, 2013) 029, arXiv:1307.0007 [hep-ph].
- [5] A. J. Larkoski, S. Marzani, and J. Thaler, “Sudakov Safety in Perturbative QCD”, *Phys. Rev. D* **91** (Jun, 2015) 111501, arXiv:1502.01719 [hep-ph].
- [6] A. J. Larkoski, J. Thaler, and W. J. Waalewijn, “Gaining (mutual) information about quark/gluon discrimination”, *JHEP* **11** (Nov, 2014) 129, arXiv:1408.3122 [hep-ph].
- [7] L. G. Almeida, S. J. Lee, G. Perez, G. F. Sterman, I. Sung, and J. Virzi, “Substructure of high- p_T Jets at the LHC”, *Phys. Rev. D* **79** (Apr, 2009) 074017, arXiv:0807.0234 [hep-ph].
- [8] C. F. Berger and G. Sterman, “Scaling rule for nonperturbative radiation in a class of event shapes”, *JHEP* **09** (Sep, 2003) 058–058, arXiv:hep-ph/0307394.
- [9] Z.-B. Kang, K. Lee, and F. Ringer, “Jet angularity measurements for single inclusive jet production”, *JHEP* **04** (Apr, 2018) 110, arXiv:1801.00790 [hep-ph].
- [10] S. Catani, G. Turnock, and B. R. Webber, “Jet broadening measures in e^+e^- annihilation”, *Phys. Lett. B* **295** (Dec, 1992) 269–276.
- [11] E. Farhi, “A QCD Test for Jets”, *Phys. Rev. Lett.* **39** (Sep, 1977) 1587–1588.
- [12] A. J. Larkoski, I. Moulton, and D. Neill, “Toward Multi-Differential Cross Sections: Measuring Two Angularities on a Single Jet”, *JHEP* **09** (Sep, 2014) 046, arXiv:1401.4458 [hep-ph].

- [13] M. Procura, W. J. Waalewijn, and L. Zeune, “Joint resummation of two angularities at next-to-next-to-leading logarithmic order”, *JHEP* **10** (Oct, 2018) 098, arXiv:1806.10622 [hep-ph].
- [14] I. W. Stewart, F. J. Tackmann, and W. J. Waalewijn, “Dissecting Soft Radiation with Factorization”, *Phys. Rev. Lett.* **114** (Mar, 2015) 092001, arXiv:1405.6722 [hep-ph].
- [15] C. Lee and G. Sterman, “Momentum flow correlations from event shapes: Factorized soft gluons and soft-collinear effective theory”, *Phys. Rev. D* **75** (Jan, 2007), arXiv:hep-ph/0611061.
- [16] H.-M. Chang, M. Procura, J. Thaler, and W. J. Waalewijn, “Calculating Track-Based Observables for the LHC”, *Phys. Rev. Lett.* **111** (Sep, 2013) 102002, arXiv:1303.6637 [hep-ph].
- [17] Z.-B. Kang, K. Lee, X. Liu, and F. Ringer, “Soft drop groomed jet angularities at the LHC”, *Phys. Lett. B* **793** (Jun, 2019) 41 – 47, arXiv:1811.06983 [hep-ph].
- [18] S. Caletti, O. Fedkevych, S. Marzani, D. Reichelt, S. Schumann, G. Soyez, and V. Theeuwes, “Jet angularities in Z+jet production at the LHC”, *JHEP* **07** (2021) 076, arXiv:2104.06920 [hep-ph].
- [19] L. G. Almeida, S. D. Ellis, C. Lee, G. Sterman, I. Sung, and J. R. Walsh, “Comparing and counting logs in direct and effective methods of QCD resummation”, *JHEP* **04** (Apr, 2014) 174, arXiv:1401.4460 [hep-ph].
- [20] G. P. Korchemsky and G. Sterman, “Power corrections to event shapes and factorization”, *Nuclear Physics B* **555** (Aug, 1999) 335–351, arXiv:hep-ph/9902341.
- [21] E.-C. Aschenauer, K. Lee, B. Page, and F. Ringer, “Jet angularities in photoproduction at the Electron-Ion Collider”, *Phys. Rev. D* **101** (Mar, 2020), arXiv:1910.11460 [hep-ph].
- [22] ALICE Collaboration, “Medium modification of the shape of small-radius jets in central Pb-Pb collisions at $\sqrt{s_{NN}} = 2.76$ TeV”, *JHEP* **10** (Oct, 2018) 139, arXiv:1807.06854 [nucl-ex].
- [23] ATLAS Collaboration, G. Aad *et al.*, “ATLAS measurements of the properties of jets for boosted particle searches”, *Phys. Rev. D* **86** (Oct, 2012) 072006, arXiv:1206.5369 [hep-ex].
- [24] CMS Collaboration, A. M. Sirunyan *et al.*, “Measurement of jet substructure observables in $t\bar{t}$ events from proton-proton collisions at $\sqrt{s} = 13$ TeV”, *Phys. Rev. D* **98** (Nov, 2018) 092014, arXiv:1808.07340 [hep-ex].
- [25] CDF Collaboration, T. Aaltonen *et al.*, “Study of Substructure of High Transverse Momentum Jets Produced in Proton-Antiproton Collisions at $\sqrt{s} = 1.96$ TeV”, *Phys. Rev. D* **85** (May, 2012) 091101, arXiv:1106.5952 [hep-ex].
- [26] ATLAS Collaboration, G. Aad *et al.*, “Jet mass and substructure of inclusive jets in $\sqrt{s} = 7$ TeV pp collisions with the ATLAS experiment”, *JHEP* **05** (May, 2012) 128, arXiv:1203.4606 [hep-ex].
- [27] ATLAS Collaboration, G. Aad *et al.*, “Measurement of the jet mass in high transverse momentum $Z(\rightarrow b\bar{b})\gamma$ production at $\sqrt{s} = 13$ TeV using the ATLAS detector”, *Phys. Lett. B* **812** (Jan, 2021) 135991, arXiv:1907.07093 [hep-ex].
- [28] ATLAS Collaboration, G. Aad *et al.*, “Measurement of soft-drop jet observables in pp collisions with the ATLAS detector at $\sqrt{s_{NN}} = 13$ TeV”, *Phys. Rev. D* **101** (Mar, 2020) 052007, arXiv:1912.09837 [hep-ex].

- [29] CMS Collaboration, A. M. Sirunyan *et al.*, “Measurement of the Jet Mass Distribution and Top Quark Mass in Hadronic Decays of Boosted Top Quarks in pp Collisions at $\sqrt{s} = 13$ TeV”, *Phys. Rev. Lett.* **124** (May, 2020) 202001, arXiv:1911.03800 [hep-ex].
- [30] CMS Collaboration, A. M. Sirunyan *et al.*, “Measurement of the groomed jet mass in Pb–Pb and pp collisions at $\sqrt{s_{NN}} = 5.02$ TeV”, *JHEP* **10** (Oct, 2018) 161, arXiv:1805.05145 [hep-ex].
- [31] CMS Collaboration, A. M. Sirunyan *et al.*, “Measurement of the jet mass in highly boosted $t\bar{t}$ events from pp collisions at $\sqrt{s} = 8$ TeV”, *Eur. Phys. J. C* **77** (Jul, 2017) 467, arXiv:1703.06330 [hep-ex].
- [32] CMS Collaboration, S. Chatrchyan *et al.*, “Studies of jet mass in dijet and W/Z + jet events”, *JHEP* **05** (May, 2013) 090, arXiv:1303.4811 [hep-ex].
- [33] CMS Collaboration, A. M. Sirunyan *et al.*, “Measurements of the differential jet cross section as a function of the jet mass in dijet events from proton-proton collisions at $\sqrt{s} = 13$ TeV”, *JHEP* **2018** (Nov, 2018) 113, arXiv:1807.05974 [hep-ex].
- [34] ATLAS Collaboration, “Measurement of $R = 0.4$ jet mass in Pb+Pb and pp collisions at $\sqrt{s_{NN}} = 5.02$ TeV with the ATLAS detector”, tech. rep., CERN, Geneva, CH, May, 2018. <https://cds.cern.ch/record/2319867>.
- [35] ATLAS Collaboration, M. Aaboud *et al.*, “Measurement of the soft-drop jet mass in pp collisions at $\sqrt{s} = 13$ TeV with the ATLAS detector”, *Phys. Rev. Lett.* **121** (Aug, 2018) 092001, arXiv:1711.08341 [hep-ex].
- [36] ALICE Collaboration, S. Acharya *et al.*, “First measurement of jet mass in Pb–Pb and p–Pb collisions at the LHC”, *Phys. Lett. B* **776** (Jan, 2018) 249–264, arXiv:1702.00804 [nucl-ex].
- [37] B. V. Jacak and B. Müller, “The exploration of hot nuclear matter”, *Science* **337** (Jul, 2012) 310–314.
- [38] B. Müller, J. Schukraft, and B. Wysłouch, “First Results from Pb+Pb Collisions at the LHC”, *Annu. Rev. Nucl. Part. S.* **62** (Nov, 2012) 361–386, arXiv:1202.3233 [hep-ex].
- [39] P. Braun-Munzinger, V. Koch, T. Schäfer, and J. Stachel, “Properties of hot and dense matter from relativistic heavy ion collisions”, *Phys. Rept.* **621** (Mar, 2016) 76–126, arXiv:1510.00442 [nucl-th]. Memorial Volume in Honor of Gerald E. Brown.
- [40] W. Busza, K. Rajagopal, and W. van der Schee, “Heavy Ion Collisions: The Big Picture, and the Big Questions”, *Annu. Rev. Nucl. Part. S.* **68** (Oct, 2018) 339–376, arXiv:1802.04801 [hep-ph].
- [41] G.-Y. Qin and X.-N. Wang, “Jet quenching in high-energy heavy-ion collisions”, *Int. J. Mod. Phys. E* **24** (Oct, 2015) 1530014, arXiv:1511.00790 [hep-ph].
- [42] J.-P. Blaizot and Y. Mehtar-Tani, “Jet structure in heavy ion collisions”, *Int. J. Mod. Phys. E* **24** (Oct, 2015) 1530012, arXiv:1503.05958 [hep-ph].
- [43] A. Majumder and M. van Leeuwen, “The theory and phenomenology of perturbative QCD based jet quenching”, *Prog. Part. Nucl. Phys.* **66** (Jan, 2011) 41 – 92, arXiv:1002.2206 [hep-ph].
- [44] J. Yan, S.-Y. Chen, W. Dai, B.-W. Zhang, and E. Wang, “Medium modifications of girth distributions for inclusive jets and $Z^0 + \text{jet}$ in relativistic heavy-ion collisions at the LHC”, *Chin. Phys. C* **45** (Feb, 2021) 024102, arXiv:2005.01093 [hep-ph].

- [45] R. Kunnawalkam Elayavalli and K. C. Zapp, “Medium response in JEWEL and its impact on jet shape observables in heavy ion collisions”, *JHEP* **07** (Jul, 2017) 141, arXiv:1707.01539 [hep-ph].
- [46] J. Casalderrey-Solana, G. Milhano, D. Pablos, and K. Rajagopal, “Modification of Jet Substructure in Heavy Ion Collisions as a Probe of the Resolution Length of Quark-Gluon Plasma”, *JHEP* **01** (Jan, 2020) 044, arXiv:1907.11248 [hep-ph].
- [47] ALICE Collaboration, S. Acharya *et al.*, “Measurements of inclusive jet spectra in pp and central Pb–Pb collisions at $\sqrt{s_{NN}} = 5.02$ TeV”, *Phys. Rev. C* **101** (Mar, 2020) 034911, arXiv:1909.09718 [nucl-ex].
- [48] J. Mulligan and M. Płoskoń, “Identifying groomed jet splittings in heavy-ion collisions”, *Phys. Rev. C* **102** (Oct, 2020) 044913, arXiv:2006.01812 [hep-ph].
- [49] T. Sjöstrand, S. Ask, J. R. Christiansen, R. Corke, N. Desai, P. Ilten, S. Mrenna, S. Prestel, C. O. Rasmussen, and P. Z. Skands, “An introduction to PYTHIA 8.2”, *Comput. Phys. Commun.* **191** (Jun, 2015) 159 – 177, arXiv:1410.3012 [hep-ph].
- [50] M. Bähr, *et al.*, “Herwig++ Physics and Manual”, *Eur. Phys. J. C* **58** (Nov, 2008) 639–707, arXiv:0803.0883 [hep-ph].
- [51] J. Bellm *et al.*, “Herwig 7.0/Herwig++ 3.0 release note”, *Eur. Phys. J. C* **76** (Apr, 2016) 196, arXiv:1512.01178 [hep-ph].
- [52] ALICE Collaboration, K. Aamodt *et al.*, “The ALICE experiment at the CERN LHC”, *JINST* **3** (Aug, 2008) .
- [53] ALICE Collaboration, B. Abelev *et al.*, “Performance of the ALICE Experiment at the CERN LHC”, *Int. J. Mod. Phys. A* **29** (Sep, 2014) 1430044, arXiv:1402.4476 [nucl-ex].
- [54] L. Evans and P. Bryant, “The CERN Large Hadron Collider: accelerator and experiments”, *JINST* **3** (Aug, 2008) S08001.
- [55] ALICE Collaboration, E. Abbas *et al.*, “Performance of the ALICE VZERO system”, *JINST* **8** (Oct, 2013) P10016, arXiv:1306.3130 [nucl-ex].
- [56] ALICE Collaboration, S. Acharya *et al.*, “ALICE 2017 luminosity determination for pp collisions at $\sqrt{s} = 5$ TeV”, ALICE-PUBLIC-2018-014. <https://cds.cern.ch/record/2648933>.
- [57] ALICE Collaboration, J. Alme *et al.*, “The ALICE TPC, a large 3-dimensional tracking device with fast readout for ultra-high multiplicity events”, *Nuclear Instruments and Methods in Physics Research Section A: Accelerators, Spectrometers, Detectors and Associated Equipment* **622** (Oct, 2010) 316–367, arXiv:1001.1950 [physics.ins-det].
- [58] ALICE Collaboration, K. Aamodt *et al.*, “Alignment of the ALICE Inner Tracking System with cosmic-ray tracks”, *JINST* **5** (Mar, 2010) P03003, arXiv:1001.0502 [physics.ins-det].
- [59] ALICE Collaboration, S. Acharya *et al.*, “Measurement of charged jet cross section in pp collisions at $\sqrt{s} = 5.02$ TeV”, *Phys. Rev. D* **100** (Dec, 2019) 092004, arXiv:1905.02536 [nucl-ex].
- [60] R. Brun, F. Bruyant, M. Maire, A. C. McPherson, and P. Zancarini, *GEANT 3: user’s guide Geant 3.10, Geant 3.11; rev. version*. CERN, Geneva, Sep, 1987. <https://cds.cern.ch/record/1119728>.

- [61] M. Cacciari, G. P. Salam, and G. Soyez, “FastJet User Manual”, *Eur. Phys. J. C* **72** (Mar, 2012) 1896, arXiv:1111.6097 [hep-ph].
- [62] M. Cacciari, G. P. Salam, and G. Soyez, “The anti- k_t jet clustering algorithm”, *JHEP* **04** (Apr, 2008) 063, arXiv:0802.1189 [hep-ph].
- [63] ALICE Collaboration, B. Abelev *et al.*, “Measurement of charged jet suppression in Pb-Pb collisions at $\sqrt{s_{NN}} = 2.76$ TeV”, *JHEP* **03** (Mar, 2014) 013, arXiv:1311.0633 [nucl-ex].
- [64] Y. Dokshitzer, G. Leder, S. Moretti, and B. Webber, “Better jet clustering algorithms”, *JHEP* **08** (Aug, 1997) 001.
- [65] P. Cal, K. Lee, F. Ringer, and W. J. Waalewijn, “Jet energy drop”, *JHEP* **2020** (Nov, 2020), arXiv:2007.12187 [hep-ph].
- [66] P. Skands, S. Carrazza, and J. Rojo, “Tuning PYTHIA 8.1: the Monash 2013 tune”, *Eur. Phys. J. C* **74** (Aug, 2014), arXiv:1404.5630 [hep-ph].
- [67] ALICE Collaboration, S. Acharya *et al.*, “The ALICE definition of primary particles”, ALICE-PUBLIC-2017-005. <https://cds.cern.ch/record/2270008>.
- [68] G. D’Agostini, “A multidimensional unfolding method based on Bayes’ theorem”, *Nuclear Instruments and Methods in Physics Research Section A: Accelerators, Spectrometers, Detectors and Associated Equipment* **362** (Jun, 1994) 487 – 498.
- [69] G. D’Agostini, “Improved iterative Bayesian unfolding”, arXiv:1010.0632 [physics.data-an].
- [70] “RooUnfold.” <https://hepunix.rl.ac.uk/~adye/software/unfold/RooUnfold.html>.
- [71] ALICE Collaboration, S. Acharya *et al.*, “Production of charged pions, kaons, and (anti-)protons in Pb-Pb and inelastic pp collisions at $\sqrt{s_{NN}} = 5.02$ TeV”, *Phys. Rev. C* **101** (Apr, 2020) 044907.
- [72] M. Dasgupta and G. P. Salam, “Resummation of nonglobal QCD observables”, *Phys. Lett. B* **512** (Jul, 2001) 323–330, arXiv:hep-ph/0104277.
- [73] C. W. Bauer, D. Pirjol, and I. W. Stewart, “Soft collinear factorization in effective field theory”, *Phys. Rev. D* **65** (Feb, 2002) 054022, arXiv:hep-ph/0109045.
- [74] H. Chen, I. Moul, X. Zhang, and H. X. Zhu, “Rethinking jets with energy correlators: Tracks, resummation, and analytic continuation”, *Phys. Rev. D* **102** (Sep, 2020) 054012, arXiv:2004.11381 [hep-ph].
- [75] Y.-T. Chien, R. Rahn, S. Schrijnder van Velzen, D. Y. Shao, W. J. Waalewijn, and B. Wu, “Recoil-free azimuthal angle for precision boson-jet correlation”, *Phys. Lett. B* **815** (Apr, 2021) 136124, arXiv:2005.12279 [hep-ph].
- [76] S. Gieseke, C. Rohr, and A. Siodmok, “Colour reconnections in Herwig++”, *Eur. Phys. J. C* **72** (Nov, 2012) 2225, arXiv:1206.0041 [hep-ph].
- [77] Z.-B. Kang, F. Ringer, and I. Vitev, “The semi-inclusive jet function in SCET and small radius resummation for inclusive jet production”, *JHEP* **10** (Oct, 2016) 125, arXiv:1606.06732 [hep-ph].
- [78] A. H. Hoang, S. Mantry, A. Pathak, and I. W. Stewart, “Nonperturbative Corrections to Soft Drop Jet Mass”, *JHEP* **12** (Dec, 2019) 002, arXiv:1906.11843 [hep-ph].

- [79] A. Pathak, I. W. Stewart, V. Vaidya, and L. Zoppi, “EFT for Soft Drop Double Differential Cross Section”, *JHEP* **04** (Apr, 2021) 32, arXiv:2012.15568 [hep-ph].
- [80] Z.-B. Kang, K. Lee, X. Liu, and F. Ringer, “The groomed and ungroomed jet mass distribution for inclusive jet production at the LHC”, *JHEP* **10** (Oct, 2018) 137, arXiv:1803.03645 [hep-ph].

A Additional figures

Figures A.1, A.2 show the groomed and ungroomed angularities for $80 < p_T^{\text{ch jet}} < 100$ GeV/c using MC generators to apply hadronization corrections.

Figures A.3, A.4 and A.5, A.6 show the groomed and ungroomed angularities using the shape function to apply hadronization corrections, for $40 < p_T^{\text{ch jet}} < 60$ GeV/c and $80 < p_T^{\text{ch jet}} < 100$ GeV/c.

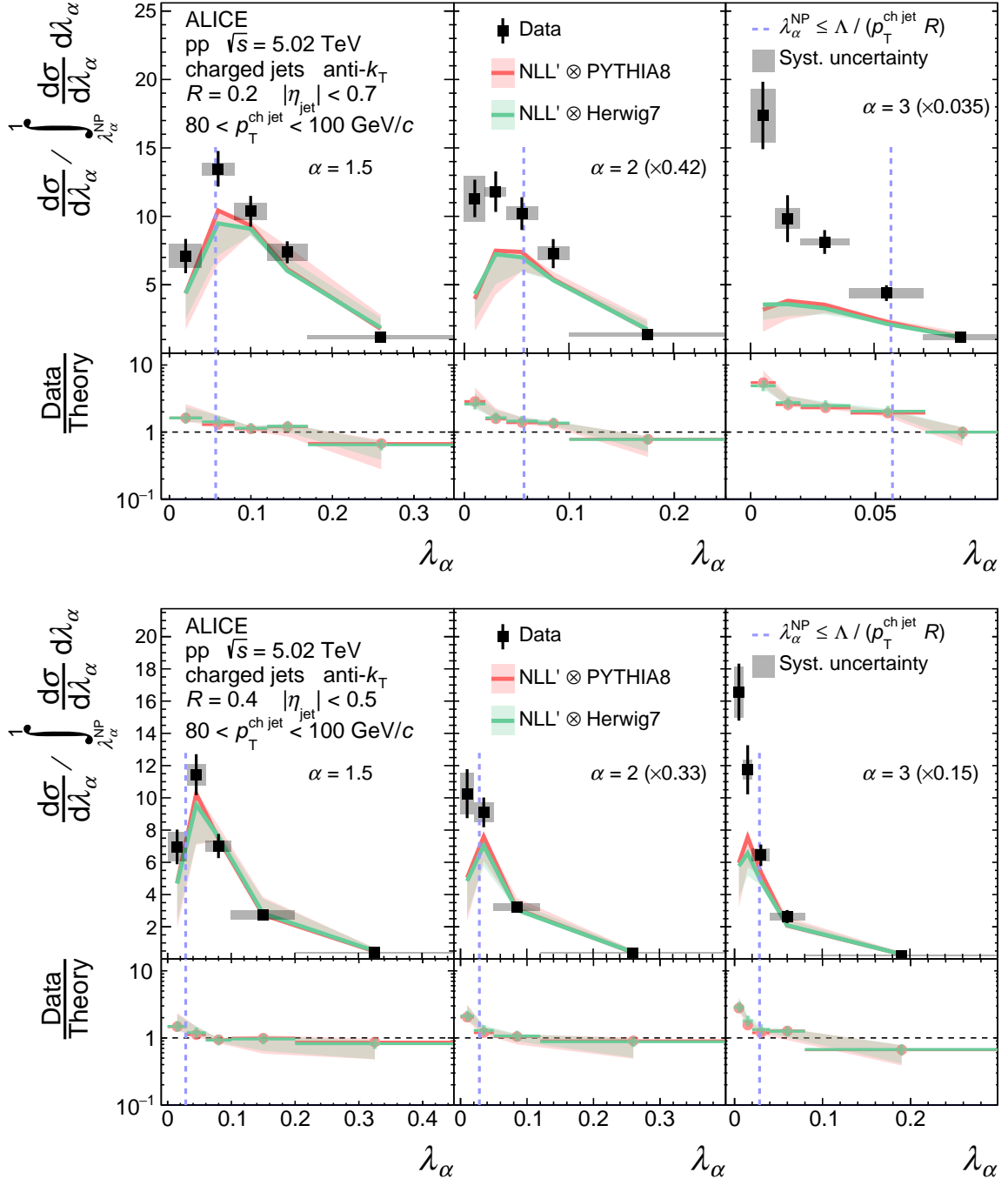


Figure A.1: Comparison of ungroomed jet angularities λ_α in pp collisions for $R = 0.2$ (top) and $R = 0.4$ (bottom) to analytical NLL' predictions with MC hadronization corrections in the range $80 < p_T^{\text{ch jet}} < 100$ GeV/c. The distributions are normalized such that the integral of the perturbative region defined by $\lambda_\alpha > \lambda_\alpha^{\text{NP}}$ (to the right of the dashed vertical line) is unity. Divided bins are placed into the left (NP) region.

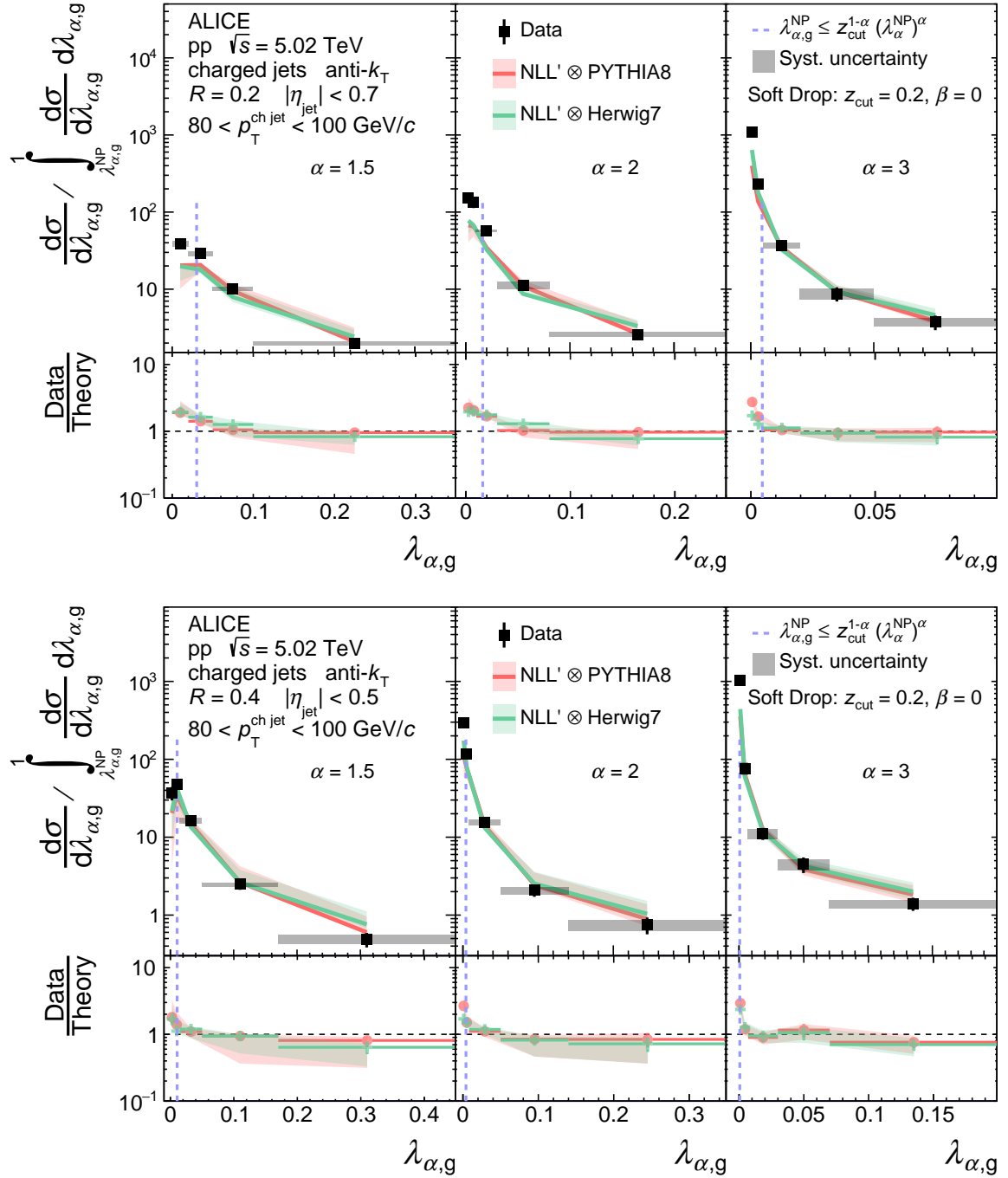


Figure A.2: Comparison of groomed jet angularities $\lambda_{\alpha,g}$ in pp collisions for $R = 0.2$ (top) and $R = 0.4$ (bottom) to analytical NLL' predictions with MC hadronization corrections in the range $80 < p_T^{\text{ch jet}} < 100$ GeV/c. The distributions are normalized such that the integral of the perturbative region defined by $\lambda_{\alpha,g} > \lambda_{\alpha,g}^{\text{NP}}$ (to the right of the dashed vertical line) is unity. Divided bins are placed into the left (NP) region.

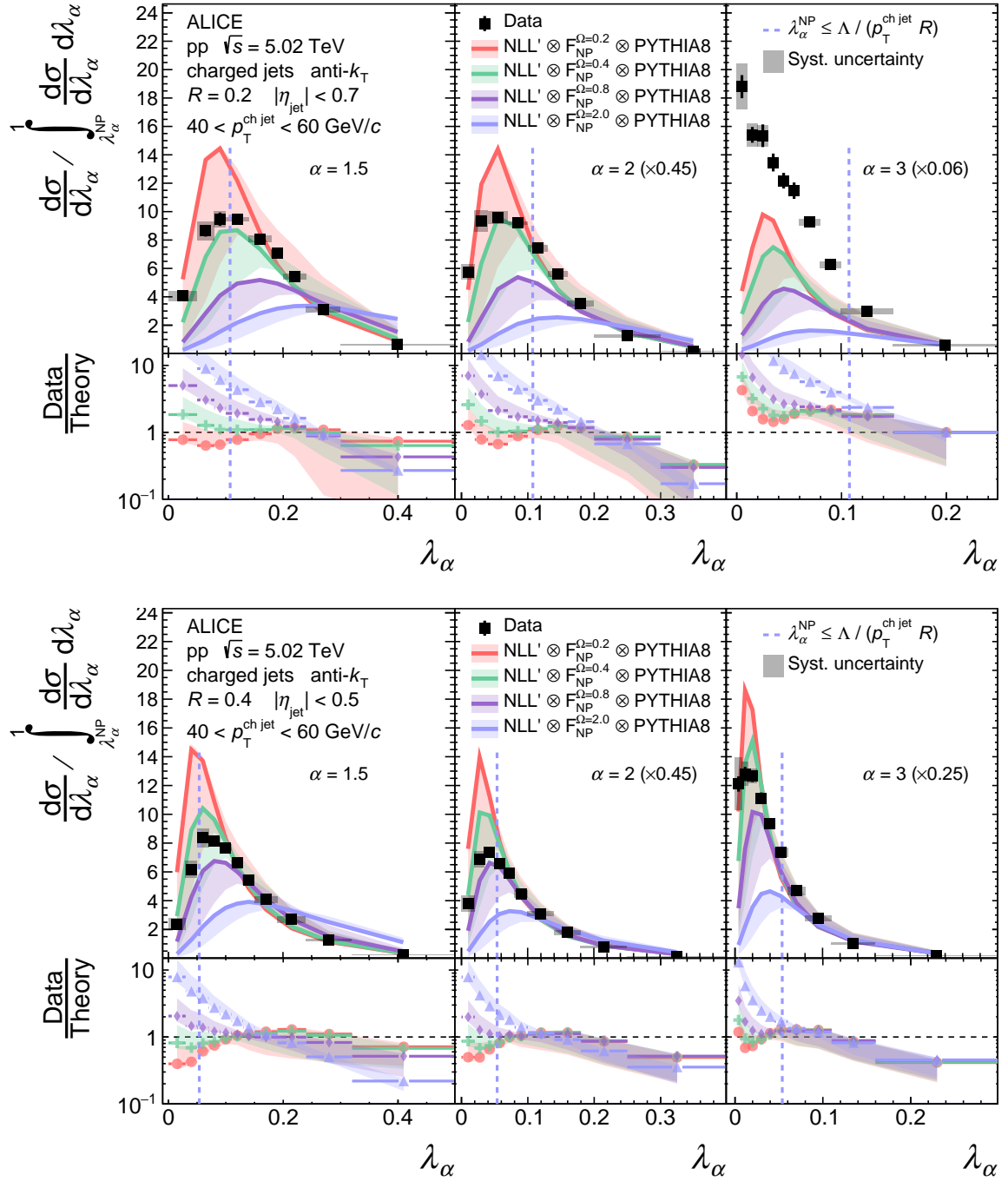


Figure A.3: Comparison of ungroomed jet angularities λ_α in pp collisions for $R = 0.2$ (top) and $R = 0.4$ (bottom) to analytical NLL' predictions using $F(k)$ convolution in the range $40 < p_T^{\text{ch,jet}} < 60$ GeV/c. The distributions are normalized such that the integral of the perturbative region defined by $\lambda_\alpha > \lambda_\alpha^{\text{NP}}$ (to the right of the dashed vertical line) is unity. Divided bins are placed into the left (NP) region.

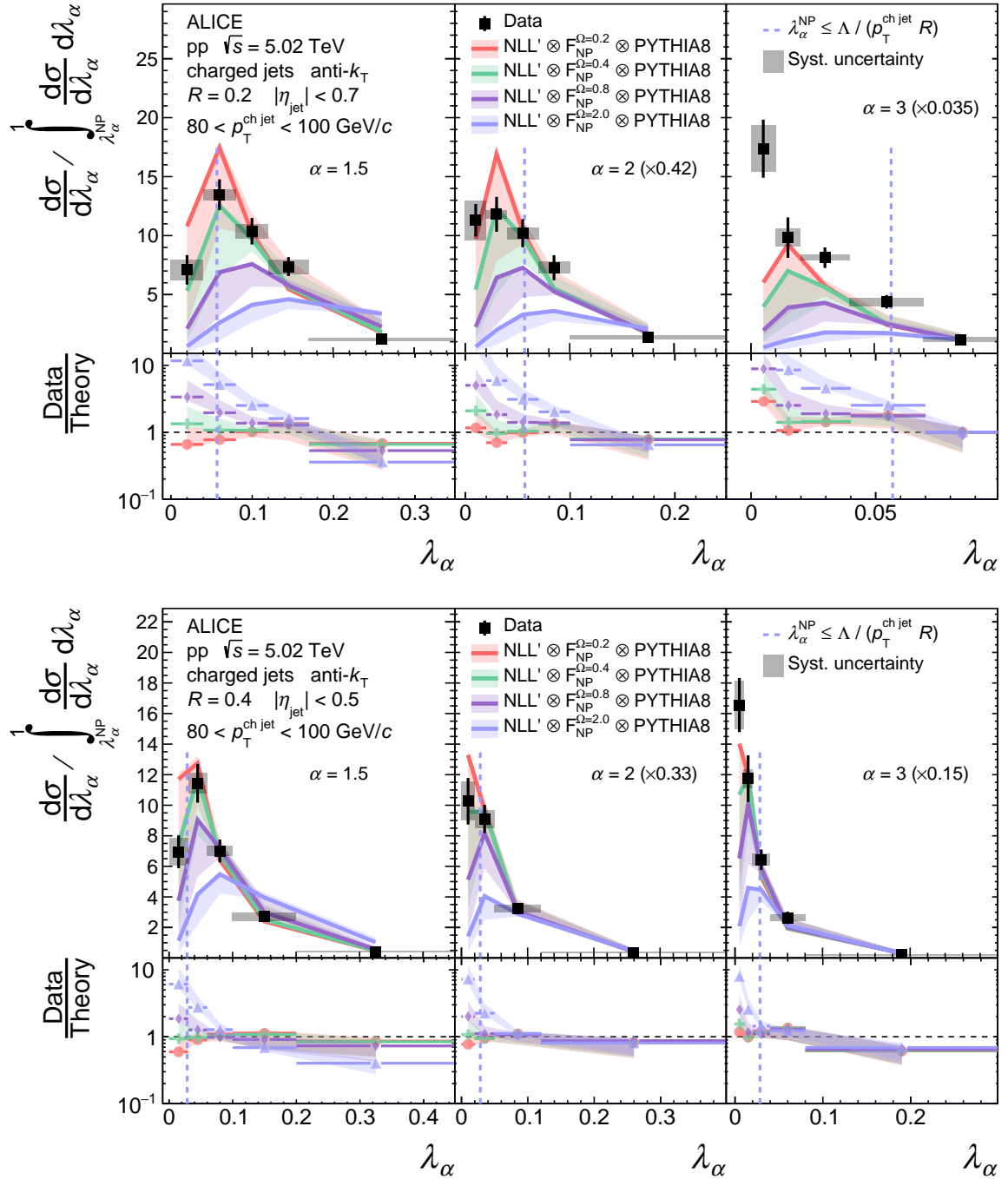


Figure A.4: Comparison of ungroomed jet angularities λ_α in pp collisions for $R = 0.2$ (top) and $R = 0.4$ (bottom) to analytical NLL' predictions using $F(k)$ convolution in the range $80 < p_T^{\text{ch,jet}} < 100$ GeV/c. The distributions are normalized such that the integral of the perturbative region defined by $\lambda_\alpha > \lambda_\alpha^{\text{NP}}$ (to the right of the dashed vertical line) is unity. Divided bins are placed into the left (NP) region.

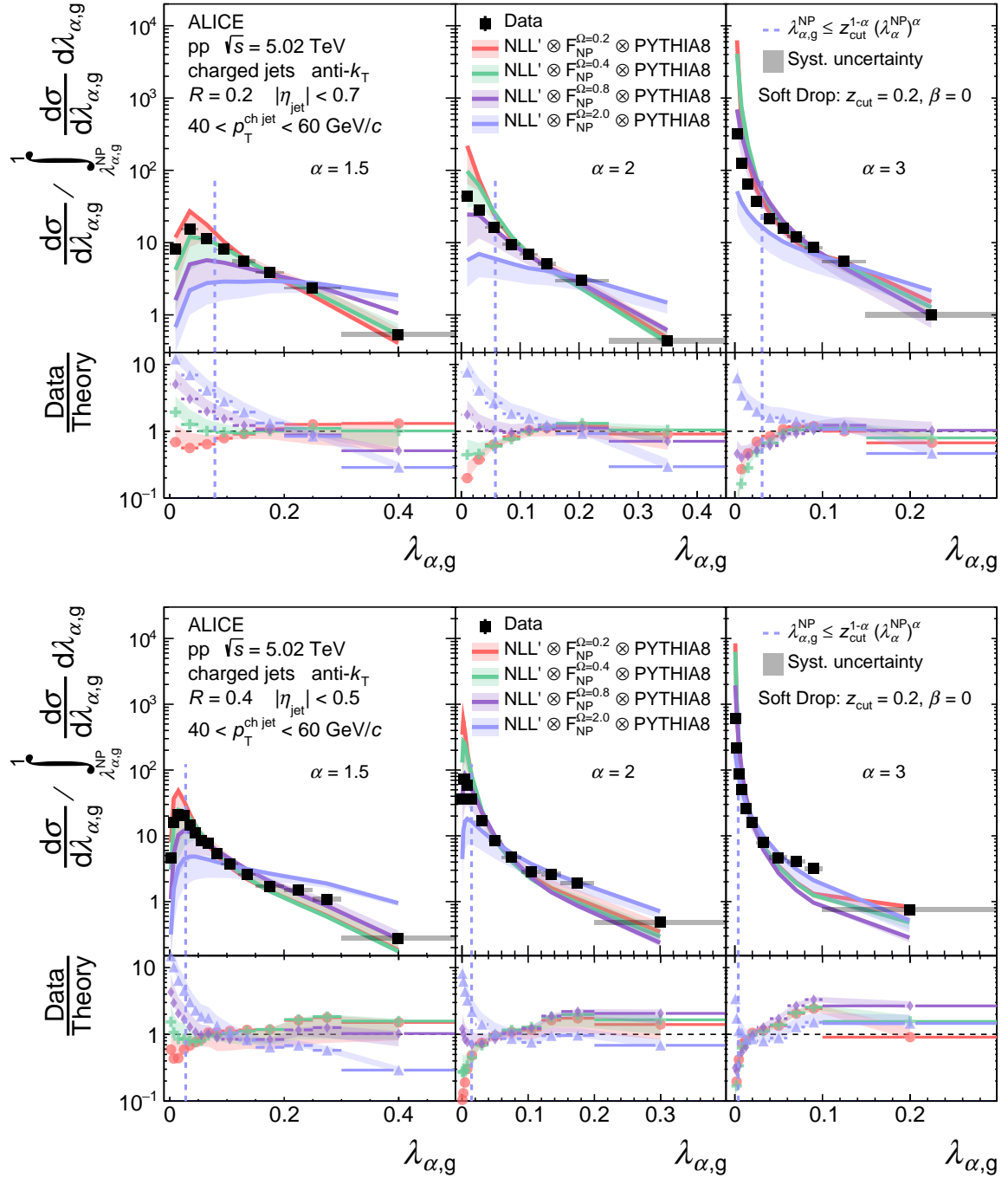


Figure A.5: Comparison of groomed jet angularities $\lambda_{\alpha,g}$ in pp collisions for $R = 0.2$ (top) and $R = 0.4$ (bottom) to analytical NLL' predictions using $F(k)$ convolution in the range $40 < p_T^{\text{ch,jet}} < 60$ GeV/c. The distributions are normalized such that the integral of the perturbative region defined by $\lambda_{\alpha,g} > \lambda_{\alpha,g}^{\text{NP}}$ (to the right of the dashed vertical line) is unity. Divided bins are placed into the left (NP) region.

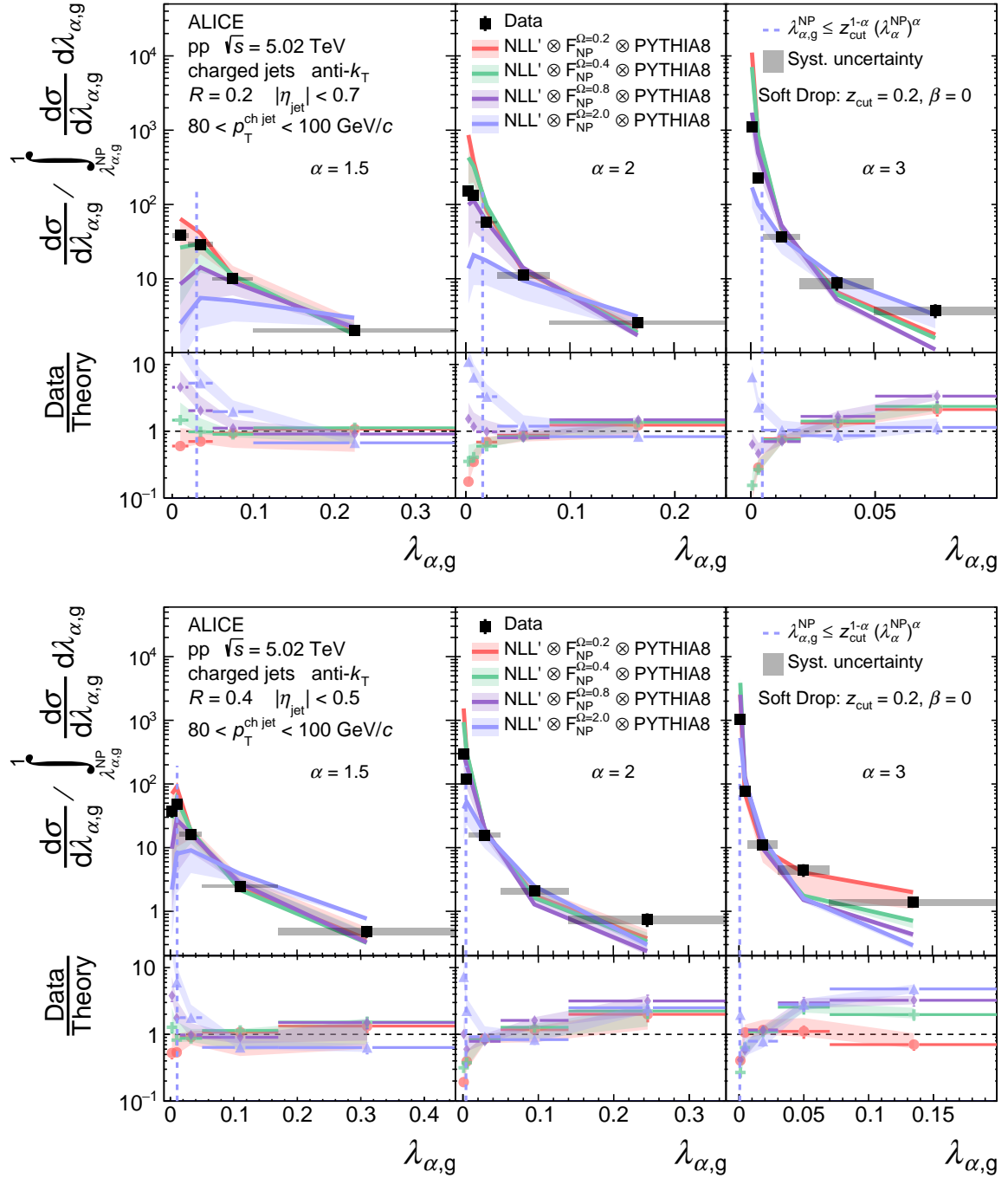


Figure A.6: Comparison of groomed jet angularities $\lambda_{\alpha,g}$ in pp collisions for $R = 0.2$ (top) and $R = 0.4$ (bottom) to analytical NLL' predictions using $F(k)$ convolution in the range $80 < p_T^{\text{ch,jet}} < 100$ GeV/c. The distributions are normalized such that the integral of the perturbative region defined by $\lambda_{\alpha,g} > \lambda_{\alpha,g}^{\text{NP}}$ (to the right of the dashed vertical line) is unity. Divided bins are placed into the left (NP) region.

B The ALICE Collaboration

S. Acharya¹⁴³, D. Adamová⁹⁸, A. Adler⁷⁶, G. Aglieri Rinella³⁵, M. Agnello³¹, N. Agrawal⁵⁵, Z. Ahammed¹⁴³, S. Ahmad¹⁶, S.U. Ahn⁷⁸, I. Ahuja³⁹, Z. Akbar⁵², A. Akindinov⁹⁵, M. Al-Turany¹¹⁰, S.N. Alam^{16,41}, D. Aleksandrov⁹¹, B. Alessandro⁶¹, H.M. Alfanda⁷, R. Alfaro Molina⁷³, B. Ali¹⁶, Y. Ali¹⁴, A. Alici²⁶, N. Alizadehvandchali¹²⁷, A. Alkin³⁵, J. Alme²¹, T. Alt⁷⁰, L. Altenkamper²¹, I. Altsybeev¹¹⁵, M.N. Anaam⁷, C. Andrei⁴⁹, D. Andreou⁹³, A. Andronic¹⁴⁶, M. Angeletti³⁵, V. Anguelov¹⁰⁷, F. Antinori⁵⁸, P. Antonioli⁵⁵, C. Anuj¹⁶, N. Apadula⁸², L. Aphecetche¹¹⁷, H. Appelshäuser⁷⁰, S. Arcelli²⁶, R. Arnaldi⁶¹, I.C. Arsene²⁰, M. Arslandok^{148,107}, A. Augustinus³⁵, R. Averbeck¹¹⁰, S. Aziz⁸⁰, M.D. Azmi¹⁶, A. Badalà⁵⁷, Y.W. Baek⁴², X. Bai^{131,110}, R. Bailhache⁷⁰, Y. Bailung⁵¹, R. Bala¹⁰⁴, A. Balbino³¹, A. Baldisseri¹⁴⁰, B. Balis², M. Ball⁴⁴, D. Banerjee⁴, R. Barbera²⁷, L. Barioglio¹⁰⁸, M. Barlou⁸⁷, G.G. Barnaföldi¹⁴⁷, L.S. Barnby⁹⁷, V. Barret¹³⁷, C. Bartels¹³⁰, K. Barth³⁵, E. Bartsch⁷⁰, F. Baruffaldi²⁸, N. Bastid¹³⁷, S. Basu⁸³, G. Batigne¹¹⁷, B. Batyunya⁷⁷, D. Bauri⁵⁰, J.L. Bazo Alba¹¹⁴, I.G. Bearden⁹², C. Beattie¹⁴⁸, I. Belikov¹³⁹, A.D.C. Bell Hechavarria¹⁴⁶, F. Bellini²⁶, R. Bellwied¹²⁷, S. Belokurova¹¹⁵, V. Belyaev⁹⁶, G. Bencedi⁷¹, S. Beole²⁵, A. Bercuci⁴⁹, Y. Berdnikov¹⁰¹, A. Berdnikova¹⁰⁷, L. Bergmann¹⁰⁷, M.G. Besoiu⁶⁹, L. Betev³⁵, P.P. Bhaduri¹⁴³, A. Bhasin¹⁰⁴, I.R. Bhat¹⁰⁴, M.A. Bhat⁴, B. Bhattacharjee⁴³, P. Bhattacharya²³, L. Bianchi²⁵, N. Bianchi⁵³, J. Bielčik³⁸, J. Bielčíková⁹⁸, J. Biernat¹²⁰, A. Bilandžić¹⁰⁸, G. Biro¹⁴⁷, S. Biswas⁴, J.T. Blair¹²¹, D. Blau⁹¹, M.B. Blidaru¹¹⁰, C. Blume⁷⁰, G. Boca^{29,59}, F. Bock⁹⁹, A. Bogdanov⁹⁶, S. Boi²³, J. Bok⁶³, L. Boldizsár¹⁴⁷, A. Bolozdynya⁹⁶, M. Bombara³⁹, P.M. Bond³⁵, G. Bonomi^{142,59}, H. Borel¹⁴⁰, A. Borissov⁸⁴, H. Bossi¹⁴⁸, E. Botta²⁵, L. Bratrud⁷⁰, P. Braun-Munzinger¹¹⁰, M. Bregant¹²³, M. Broz³⁸, G.E. Bruno^{109,34}, M.D. Buckland¹³⁰, D. Budnikov¹¹¹, H. Buesching⁷⁰, S. Bufalino³¹, O. Bugnon¹¹⁷, P. Buhler¹¹⁶, Z. Buthelezi^{74,134}, J.B. Butt¹⁴, S.A. Bysiak¹²⁰, M. Cai^{28,7}, H. Caines¹⁴⁸, A. Caliva¹¹⁰, E. Calvo Villar¹¹⁴, J.M.M. Camacho¹²², R.S. Camacho⁴⁶, P. Camerini²⁴, F.D.M. Canedo¹²³, F. Carnesecchi^{35,26}, R. Caron¹⁴⁰, J. Castillo Castellanos¹⁴⁰, E.A.R. Casula²³, F. Catalano³¹, C. Ceballos Sanchez⁷⁷, P. Chakraborty⁵⁰, S. Chandra¹⁴³, S. Chapeland³⁵, M. Chartier¹³⁰, S. Chattopadhyay¹⁴³, S. Chattopadhyay¹¹², A. Chauvin²³, T.G. Chavez⁴⁶, T. Cheng⁷, C. Cheshkov¹³⁸, B. Cheynis¹³⁸, V. Chibante Barroso³⁵, D.D. Chinellato¹²⁴, S. Cho⁶³, P. Chochula³⁵, P. Christakoglou⁹³, C.H. Christensen⁹², P. Christiansen⁸³, T. Chujo¹³⁶, C. Cicalo⁵⁶, L. Cifarelli²⁶, F. Cindolo⁵⁵, M.R. Ciupek¹¹⁰, G. Clai^{II,55}, J. Cleymans^{I,126}, F. Colamaria⁵⁴, J.S. Colburn¹¹³, D. Colella^{109,54,34,147}, A. Collu⁸², M. Colocci³⁵, M. Concas^{III,61}, G. Conesa Balbastre⁸¹, Z. Conesa del Valle⁸⁰, G. Contin²⁴, J.G. Contreras³⁸, M.L. Coquet¹⁴⁰, T.M. Cormier⁹⁹, P. Cortese³², M.R. Cosentino¹²⁵, F. Costa³⁵, S. Costanza^{29,59}, P. Crochet¹³⁷, R. Cruz-Torres⁸², E. Cuautle⁷¹, P. Cui⁷, L. Cunqueiro⁹⁹, A. Dainese⁵⁸, M.C. Danisch¹⁰⁷, A. Danu⁶⁹, I. Das¹¹², P. Das⁸⁹, P. Das⁴, S. Das⁴, S. Dash⁵⁰, S. De⁸⁹, A. De Caro³⁰, G. de Cataldo⁵⁴, L. De Cilladi²⁵, J. de Cuveland⁴⁰, A. De Falco²³, D. De Gruttola³⁰, N. De Marco⁶¹, C. De Martin²⁴, S. De Pasquale³⁰, S. Deb⁵¹, H.F. Degenhardt¹²³, K.R. Deja¹⁴⁴, L. Dello Stritto³⁰, S. Delsanto²⁵, W. Deng⁷, P. Dhankher¹⁹, D. Di Bari³⁴, A. Di Mauro³⁵, R.A. Diaz⁸, T. Dietel¹²⁶, Y. Ding^{138,7}, R. Divià³⁵, D.U. Dixit¹⁹, Ø. Djuvsland²¹, U. Dmitrieva⁶⁵, J. Do⁶³, A. Dobrin⁶⁹, B. Dönigus⁷⁰, O. Dordic²⁰, A.K. Dubey¹⁴³, A. Dubla^{110,93}, S. Dudi¹⁰³, M. Dukhishyam⁸⁹, P. Dupieux¹³⁷, N. Dzalaiova¹³, T.M. Eder¹⁴⁶, R.J. Ehlers⁹⁹, V.N. Eikeland²¹, F. Eisenhut⁷⁰, D. Elia⁵⁴, B. Erasmus¹¹⁷, F. Ercolessi²⁶, F. Erhardt¹⁰², A. Erokhin¹¹⁵, M.R. Ersdal²¹, B. Espagnon⁸⁰, G. Eulisse³⁵, D. Evans¹¹³, S. Evdokimov⁹⁴, L. Fabbietti¹⁰⁸, M. Faggin²⁸, J. Faivre⁸¹, F. Fan⁷, A. Fantoni⁵³, M. Fasel⁹⁹, P. Fedichio³¹, A. Feliciello⁶¹, G. Feofilov¹¹⁵, A. Fernández Téllez⁴⁶, A. Ferrero¹⁴⁰, A. Ferretti²⁵, V.J.G. Feuillard¹⁰⁷, J. Figiel¹²⁰, S. Filchagin¹¹¹, D. Finogeev⁶⁵, F.M. Fionda^{56,21}, G. Fiorenza^{35,109}, F. Flor¹²⁷, A.N. Flores¹²¹, S. Foertsch⁷⁴, P. Foka¹¹⁰, S. Fokin⁹¹, E. Fragiaco⁶², E. Frajna¹⁴⁷, U. Fuchs³⁵, N. Funicello³⁰, C. Furget⁸¹, A. Furs⁶⁵, J.J. Gaardhøje⁹², M. Gagliardi²⁵, A.M. Gago¹¹⁴, A. Gal¹³⁹, C.D. Galvan¹²², P. Ganoti⁸⁷, C. Garabatos¹¹⁰, J.R.A. Garcia⁴⁶, E. Garcia-Solis¹⁰, K. Garg¹¹⁷, C. Gargiulo³⁵, A. Garibli⁹⁰, K. Garner¹⁴⁶, P. Gasik¹¹⁰, E.F. Gauger¹²¹, A. Gautam¹²⁹, M.B. Gay Ducati⁷², M. Germain¹¹⁷, P. Ghosh¹⁴³, S.K. Ghosh⁴, M. Giacalone²⁶, P. Gianotti⁵³, P. Giubellino^{110,61}, P. Giubilato²⁸, A.M.C. Glaenger¹⁴⁰, P. Glässel¹⁰⁷, D.J.Q. Goh⁸⁵, V. Gonzalez¹⁴⁵, L.H. González-Trueba⁷³, S. Gorbunov⁴⁰, M. Gorgon², L. Görlich¹²⁰, S. Gotovac³⁶, V. Grabski⁷³, L.K. Graczykowski¹⁴⁴, L. Greiner⁸², A. Grelli⁶⁴, C. Grigoras³⁵, V. Grigoriev⁹⁶, A. Grigoryan^{I,1}, S. Grigoryan^{77,1}, O.S. Groettvik²¹, F. Grosa^{35,61}, J.F. Grosse-Oetringhaus³⁵, R. Grosso¹¹⁰, G.G. Guardiano¹²⁴, R. Guernane⁸¹, M. Guilbaud¹¹⁷, K. Gulbrandsen⁹², T. Gunji¹³⁵, W. Guo⁷, A. Gupta¹⁰⁴, R. Gupta¹⁰⁴, S.P. Guzman⁴⁶, L. Gyulai¹⁴⁷, M.K. Habib¹¹⁰, C. Hadjidakis⁸⁰, G. Halimoglu⁷⁰, H. Hamagaki⁸⁵, G. Hamar¹⁴⁷, M. Hamid⁷, R. Hannigan¹²¹, M.R. Haque^{144,89}, A. Harlanderova¹¹⁰, J.W. Harris¹⁴⁸, A. Harton¹⁰, J.A. Hasenbichler³⁵, H. Hassan⁹⁹, D. Hatzifotiadou⁵⁵, P. Hauer⁴⁴, L.B. Havener¹⁴⁸, S. Hayashi¹³⁵, S.T. Heckel¹⁰⁸, E. Hellbär¹¹⁰, H. Helstrup³⁷, T. Herman³⁸, E.G. Hernandez⁴⁶, G. Herrera Corral⁹, F. Herrmann¹⁴⁶, K.F. Hetland³⁷, H. Hillemanns³⁵, C. Hills¹³⁰, B. Hippolyte¹³⁹, B. Hofman⁶⁴, B. Hohlweger⁹³, J. Honeremann¹⁴⁶, G.H. Hong¹⁴⁹, D. Horak³⁸, S. Hornung¹¹⁰, A. Horzyk², R. Hosokawa¹⁵, Y. Hou⁷, P. Hristov³⁵, C. Hughes¹³³, P. Huhn⁷⁰, T.J. Humanic¹⁰⁰, H. Hushnud¹¹², L.A. Husova¹⁴⁶, A. Hutson¹²⁷, D. Hutter⁴⁰, J.P. Iddon^{35,130}, R. Ilkaev¹¹¹, H. Ilyas¹⁴, M. Inaba¹³⁶,

G.M. Innocenti³⁵, M. Ippolitov⁹¹, A. Isakov^{38,98}, M.S. Islam¹¹², M. Ivanov¹¹⁰, V. Ivanov¹⁰¹, V. Izucheev⁹⁴, M. Jablonski², B. Jacak⁸², N. Jacazio³⁵, P.M. Jacobs⁸², S. Jadlovská¹¹⁹, J. Jadlovsky¹¹⁹, S. Jaelani⁶⁴, C. Jahnke^{124,123}, M.J. Jakubowska¹⁴⁴, A. Jalotra¹⁰⁴, M.A. Janik¹⁴⁴, T. Janson⁷⁶, M. Jercic¹⁰², O. Jevons¹¹³, A.A.P. Jimenez⁷¹, F. Jonas^{99,146}, P.G. Jones¹¹³, J.M. Jowett^{35,110}, J. Jung⁷⁰, M. Jung⁷⁰, A. Junique³⁵, A. Jusko¹¹³, J. Kaewjai¹¹⁸, P. Kalinak⁶⁶, A. Kalweit³⁵, V. Kaplin⁹⁶, S. Kar⁷, A. Karasu Uysal⁷⁹, D. Karatovic¹⁰², O. Karavichev⁶⁵, T. Karavicheva⁶⁵, P. Karczmarczyk¹⁴⁴, E. Karpechev⁶⁵, A. Kazantsev⁹¹, U. Kebschull⁷⁶, R. Keidel⁴⁸, D.L.D. Keijdener⁶⁴, M. Keil³⁵, B. Ketzer⁴⁴, Z. Khabanova⁹³, A.M. Khan⁷, S. Khan¹⁶, A. Khanzadeev¹⁰¹, Y. Kharlov⁹⁴, A. Khatun¹⁶, A. Khuntia¹²⁰, B. Kileng³⁷, B. Kim^{17,63}, C. Kim¹⁷, D.J. Kim¹²⁸, E.J. Kim⁷⁵, J. Kim¹⁴⁹, J.S. Kim⁴², J. Kim¹⁰⁷, J. Kim¹⁴⁹, J. Kim⁷⁵, M. Kim¹⁰⁷, S. Kim¹⁸, T. Kim¹⁴⁹, S. Kirsch⁷⁰, I. Kisel⁴⁰, S. Kiselev⁹⁵, A. Kisiel¹⁴⁴, J.P. Kitowski², J.L. Klay⁶, J. Klein³⁵, S. Klein⁸², C. Klein-Bösing¹⁴⁶, M. Kleiner⁷⁰, T. Klemenz¹⁰⁸, A. Kluge³⁵, A.G. Knospe¹²⁷, C. Kobdaj¹¹⁸, M.K. Köhler¹⁰⁷, T. Kollegger¹¹⁰, A. Kondratyev⁷⁷, N. Kondratyeva⁹⁶, E. Kondratyuk⁹⁴, J. König⁷⁰, S.A. Königstorfer¹⁰⁸, P.J. Konopka^{35,2}, G. Kornakov¹⁴⁴, S.D. Koryciak², L. Koska¹¹⁹, A. Kotliarov⁹⁸, O. Kovalenko⁸⁸, V. Kovalenko¹¹⁵, M. Kowalski¹²⁰, I. Králik⁶⁶, A. Kravčáková³⁹, L. Kreis¹¹⁰, M. Krivda^{113,66}, F. Krizek⁹⁸, K. Krizkova Gajdosova³⁸, M. Kroesen¹⁰⁷, M. Krüger⁷⁰, E. Kryshen¹⁰¹, M. Krzewicki⁴⁰, V. Kučera³⁵, C. Kuhn¹³⁹, P.G. Kuijer⁹³, T. Kumaoka¹³⁶, D. Kumar¹⁴³, L. Kumar¹⁰³, N. Kumar¹⁰³, S. Kundu^{35,89}, P. Kurashvili⁸⁸, A. Kurepin⁶⁵, A.B. Kurepin⁶⁵, A. Kuryakin¹¹¹, S. Kushpil⁹⁸, J. Kvapil¹¹³, M.J. Kweon⁶³, J.Y. Kwon⁶³, Y. Kwon¹⁴⁹, S.L. La Pointe⁴⁰, P. La Rocca²⁷, Y.S. Lai⁸², A. Lakrathok¹¹⁸, M. Lamanna³⁵, R. Langoy¹³², K. Lapidus³⁵, P. Larionov^{35,53}, E. Laudi³⁵, L. Lautner^{35,108}, R. Lavicka³⁸, T. Lazareva¹¹⁵, R. Lea^{142,24,59}, J. Lehrbach⁴⁰, R.C. Lemmon⁹⁷, I. León Monzón¹²², E.D. Lesser¹⁹, M. Lettrich^{35,108}, P. Lévai¹⁴⁷, X. Li¹¹, X.L. Li⁷, J. Lien¹³², R. Lietava¹¹³, B. Lim¹⁷, S.H. Lim¹⁷, V. Lindenstruth⁴⁰, A. Lindner⁴⁹, C. Lippmann¹¹⁰, A. Liu¹⁹, D.H. Liu⁷, J. Liu¹³⁰, I.M. Lofnes²¹, V. Loginov⁹⁶, C. Loizides⁹⁹, P. Loncar³⁶, J.A. Lopez¹⁰⁷, X. Lopez¹³⁷, E. López Torres⁸, J.R. Luhder¹⁴⁶, M. Lunardon²⁸, G. Luparello⁶², Y.G. Ma⁴¹, A. Maevskaya⁶⁵, M. Mager³⁵, T. Mahmoud⁴⁴, A. Maire¹³⁹, M. Malaev¹⁰¹, N.M. Malik¹⁰⁴, Q.W. Malik²⁰, L. Malinina^{IV,77}, D. Mal'Kevich⁹⁵, N. Mallick⁵¹, P. Malzacher¹¹⁰, G. Mandaglio^{33,57}, V. Manko⁹¹, F. Manso¹³⁷, V. Manzari⁵⁴, Y. Mao⁷, J. Mares⁶⁸, G.V. Margagliotti²⁴, A. Margotti⁵⁵, A. Marín¹¹⁰, C. Markert¹²¹, M. Marquard⁷⁰, N.A. Martin¹⁰⁷, P. Martinengo³⁵, J.L. Martinez¹²⁷, M.I. Martínez⁴⁶, G. Martínez García¹¹⁷, S. Masciocchi¹¹⁰, M. Masera²⁵, A. Masoni⁵⁶, L. Massacrier⁸⁰, A. Mastroserio^{141,54}, A.M. Mathis¹⁰⁸, O. Matonoha⁸³, P.F.T. Matuoka¹²³, A. Matyja¹²⁰, C. Mayer¹²⁰, A.L. Mazuecos³⁵, F. Mazzaschi²⁵, M. Mazzilli³⁵, M.A. Mazzoni^{I,60}, J.E. Mdhuli¹³⁴, A.F. Mechler⁷⁰, F. Meddi²², Y. Melikyan⁶⁵, A. Menchaca-Rocha⁷³, E. Meninno^{116,30}, A.S. Menon¹²⁷, M. Meres¹³, S. Mhlanga^{126,74}, Y. Miake¹³⁶, L. Micheletti^{61,25}, L.C. Migliorin¹³⁸, D.L. Mihaylov¹⁰⁸, K. Mikhaylov^{77,95}, A.N. Mishra¹⁴⁷, D. Miśkowiec¹¹⁰, A. Modak⁴, A.P. Mohanty⁶⁴, B. Mohanty⁸⁹, M. Mohisin Khan^{V,16}, M.A. Molander⁴⁵, Z. Moravcova⁹², C. Mordasini¹⁰⁸, D.A. Moreira De Godoy¹⁴⁶, L.A.P. Moreno⁴⁶, I. Morozov⁶⁵, A. Morsch³⁵, T. Mrnjavac³⁵, V. Muccifora⁵³, E. Mudnic³⁶, D. Mühlheim¹⁴⁶, S. Muhuri¹⁴³, J.D. Mulligan⁸², A. Mulliri²³, M.G. Munhoz¹²³, R.H. Munzer⁷⁰, H. Murakami¹³⁵, S. Murray¹²⁶, L. Musa³⁵, J. Musinsky⁶⁶, J.W. Myrcha¹⁴⁴, B. Naik^{134,50}, R. Nair⁸⁸, B.K. Nandi⁵⁰, R. Nania⁵⁵, E. Nappi⁵⁴, M.U. Naru¹⁴, A.F. Nassirpour⁸³, A. Nath¹⁰⁷, C. Nattrass¹³³, A. Neagu²⁰, L. Nellen⁷¹, S.V. Nesbo³⁷, G. Neskovic⁴⁰, D. Nesterov¹¹⁵, B.S. Nielsen⁹², S. Nikolaev⁹¹, S. Nikulin⁹¹, V. Nikulin¹⁰¹, F. Noferini⁵⁵, S. Noh¹², P. Nomokonov⁷⁷, J. Norman¹³⁰, N. Novitzky¹³⁶, P. Nowakowski¹⁴⁴, A. Nyman⁹¹, J. Nystrand²¹, M. Ogino⁸⁵, A. Ohlson⁸³, V.A. Okorokov⁹⁶, J. Oleniacz¹⁴⁴, A.C. Oliveira Da Silva¹³³, M.H. Oliver¹⁴⁸, A. Onnerstad¹²⁸, C. Oppedisano⁶¹, A. Ortiz Velasquez⁷¹, T. Osako⁴⁷, A. Oskarsson⁸³, J. Otwinowski¹²⁰, K. Oyama⁸⁵, Y. Pachmayer¹⁰⁷, S. Padhan⁵⁰, D. Pagano^{142,59}, G. Paic⁷¹, A. Palasciano⁵⁴, J. Pan¹⁴⁵, S. Panebianco¹⁴⁰, P. Pareek¹⁴³, J. Park⁶³, J.E. Parkkila¹²⁸, S.P. Pathak¹²⁷, R.N. Patra^{104,35}, B. Paul²³, H. Pei⁷, T. Peitzmann⁶⁴, X. Peng⁷, L.G. Pereira⁷², H. Pereira Da Costa¹⁴⁰, D. Peresunko⁹¹, G.M. Perez⁸, S. Perrin¹⁴⁰, Y. Pestov⁵, V. Petráček³⁸, M. Petrovici⁴⁹, R.P. Pezzi^{117,72}, S. Piano⁶², M. Pikna¹³, P. Pillot¹¹⁷, O. Pinazza^{55,35}, L. Pinsky¹²⁷, C. Pinto²⁷, S. Pisano⁵³, M. Płoskoń⁸², M. Planinic¹⁰², F. Pliquett⁷⁰, M.G. Poghosyan⁹⁹, B. Polichtchouk⁹⁴, S. Politano³¹, N. Poljak¹⁰², A. Pop⁴⁹, S. Porteboeuf-Houssais¹³⁷, J. Porter⁸², V. Pozdniakov⁷⁷, S.K. Prasad⁴, R. Preghenella⁵⁵, F. Prino⁶¹, C.A. Pruneau¹⁴⁵, I. Pshenichnov⁶⁵, M. Puccio³⁵, S. Qiu⁹³, L. Quaglia²⁵, R.E. Quishpe¹²⁷, S. Ragoni¹¹³, A. Rakotozafindrabe¹⁴⁰, L. Ramello³², F. Rami¹³⁹, S.A.R. Ramirez⁴⁶, A.G.T. Ramos³⁴, T.A. Rancien⁸¹, R. Raniwala¹⁰⁵, S. Raniwala¹⁰⁵, S.S. Räsänen⁴⁵, R. Rath⁵¹, I. Ravasenga⁹³, K.F. Read^{99,133}, A.R. Redelbach⁴⁰, K. Redlich^{VI,88}, A. Rehman²¹, P. Reichelt⁷⁰, F. Reidt³⁵, H.A. Reme-ness³⁷, R. Renfordt⁷⁰, Z. Rescakova³⁹, K. Reygers¹⁰⁷, A. Riabov¹⁰¹, V. Riabov¹⁰¹, T. Richert⁸³, M. Richter²⁰, W. Riegler³⁵, F. Riggi²⁷, C. Ristea⁶⁹, M. Rodríguez Cahuantzi⁴⁶, K. Røed²⁰, R. Rogalev⁹⁴, E. Rogochaya⁷⁷, T.S. Rogoschinski⁷⁰, D. Rohr³⁵, D. Röhrich²¹, P.F. Rojas⁴⁶, P.S. Rokita¹⁴⁴, F. Ronchetti⁵³, A. Rosano^{33,57}, E.D. Rosas⁷¹, A. Rossi⁵⁸, A. Rotondi^{29,59}, A. Roy⁵¹, P. Roy¹¹², S. Roy⁵⁰, N. Rubini²⁶, O.V. Rueda⁸³, R. Rui²⁴, B. Ruyantsev⁷⁷, P.G. Russek², A. Rustamov⁹⁰, E. Ryabinkin⁹¹, Y. Ryabov¹⁰¹, A. Rybicki¹²⁰, H. Rytönen¹²⁸, W. Rzeska¹⁴⁴,

O.A.M. Saarimaki⁴⁵, R. Sadek¹¹⁷, S. Sadovsky⁹⁴, J. Saetre²¹, K. Šafařík³⁸, S.K. Saha¹⁴³, S. Saha⁸⁹, B. Sahoo⁵⁰, P. Sahoo⁵⁰, R. Sahoo⁵¹, S. Sahoo⁶⁷, D. Sahu⁵¹, P.K. Sahu⁶⁷, J. Saini¹⁴³, S. Sakai¹³⁶, S. Sambyal¹⁰⁴, V. Samsonov^{1,101,96}, D. Sarkar¹⁴⁵, N. Sarkar¹⁴³, P. Sarma⁴³, V.M. Sarti¹⁰⁸, M.H.P. Sas¹⁴⁸, J. Schambach^{99,121}, H.S. Scheid⁷⁰, C. Schiaua⁴⁹, R. Schicker¹⁰⁷, A. Schmah¹⁰⁷, C. Schmidt¹¹⁰, H.R. Schmidt¹⁰⁶, M.O. Schmidt³⁵, M. Schmidt¹⁰⁶, N.V. Schmidt^{99,70}, A.R. Schmier¹³³, R. Schotter¹³⁹, J. Schukraft³⁵, Y. Schutz¹³⁹, K. Schwarz¹¹⁰, K. Schweda¹¹⁰, G. Scioli²⁶, E. Scomparin⁶¹, J.E. Seger¹⁵, Y. Sekiguchi¹³⁵, D. Sekihata¹³⁵, I. Selyuzhenkov^{110,96}, S. Senyukov¹³⁹, J.J. Seo⁶³, D. Serebryakov⁶⁵, L. Šerkšnyte¹⁰⁸, A. Sevcenco⁶⁹, T.J. Shaba⁷⁴, A. Shabanov⁶⁵, A. Shabetai¹¹⁷, R. Shahoyan³⁵, W. Shaikh¹¹², A. Shangaraev⁹⁴, A. Sharma¹⁰³, H. Sharma¹²⁰, M. Sharma¹⁰⁴, N. Sharma¹⁰³, S. Sharma¹⁰⁴, U. Sharma¹⁰⁴, O. Sheibani¹²⁷, K. Shigaki⁴⁷, M. Shimomura⁸⁶, S. Shirinkin⁹⁵, Q. Shou⁴¹, Y. Sibiriak⁹¹, S. Siddhanta⁵⁶, T. Siemiarczuk⁸⁸, T.F. Silva¹²³, D. Silvermyr⁸³, G. Simonetti³⁵, B. Singh¹⁰⁸, R. Singh⁸⁹, R. Singh¹⁰⁴, R. Singh⁵¹, V.K. Singh¹⁴³, V. Singhal¹⁴³, T. Sinha¹¹², B. Sitar¹³, M. Sitta³², T.B. Skaali²⁰, G. Skorodumovs¹⁰⁷, M. Slupecki⁴⁵, N. Smirnov¹⁴⁸, R.J.M. Snellings⁶⁴, C. Soncco¹¹⁴, J. Song¹²⁷, A. Songmoolnak¹¹⁸, F. Soramel²⁸, S. Sorensen¹³³, I. Sputowska¹²⁰, J. Stachel¹⁰⁷, I. Stan⁶⁹, P.J. Steffanic¹³³, S.F. Stiefelmaier¹⁰⁷, D. Stocco¹¹⁷, I. Storehaug²⁰, M.M. Storetvedt³⁷, C.P. Stylianidis⁹³, A.A.P. Suaide¹²³, T. Sugitate⁴⁷, C. Suire⁸⁰, M. Sukhanov⁶⁵, M. Suljic³⁵, R. Sultanov⁹⁵, M. Šumbera⁹⁸, V. Sumberia¹⁰⁴, S. Sumowidagdo⁵², S. Swain⁶⁷, A. Szabo¹³, I. Szarka¹³, U. Tabassam¹⁴, S.F. Taghavi¹⁰⁸, G. Taillepiet¹³⁷, J. Takahashi¹²⁴, G.J. Tambave²¹, S. Tang^{137,7}, Z. Tang¹³¹, M. Tarhini¹¹⁷, M.G. Tarzila⁴⁹, A. Tauro³⁵, G. Tejada Muñoz⁴⁶, A. Telesca³⁵, L. Terlizzi²⁵, C. Terrevoli¹²⁷, G. Tersimonov³, S. Thakur¹⁴³, D. Thomas¹²¹, R. Tieulent¹³⁸, A. Tikhonov⁶⁵, A.R. Timmins¹²⁷, M. Tkacik¹¹⁹, A. Toia⁷⁰, N. Topilskaya⁶⁵, M. Toppi⁵³, F. Torales-Acosta¹⁹, T. Tork⁸⁰, S.R. Torres³⁸, A. Trifiró^{33,57}, S. Tripathy^{55,71}, T. Tripathy⁵⁰, S. Trogolo^{35,28}, G. Trombetta³⁴, V. Trubnikov³, W.H. Trzaska¹²⁸, T.P. Trzcinski¹⁴⁴, B.A. Trzeciak³⁸, A. Tumkin¹¹¹, R. Turrisi⁵⁸, T.S. Tveter²⁰, K. Ullaland²¹, A. Uras¹³⁸, M. Urioni^{59,142}, G.L. Usai²³, M. Vala³⁹, N. Valle^{59,29}, S. Vallero⁶¹, N. van der Kolk⁶⁴, L.V.R. van Doremalen⁶⁴, M. van Leeuwen⁹³, R.J.G. van Weelden⁹³, P. Vande Vyvre³⁵, D. Varga¹⁴⁷, Z. Varga¹⁴⁷, M. Varga-Kofarago¹⁴⁷, A. Vargas⁴⁶, M. Vasileiou⁸⁷, A. Vasiliev⁹¹, O. Vázquez Doce^{53,108}, V. Vechernin¹¹⁵, E. Vercellin²⁵, S. Vergara Limón⁴⁶, L. Vermunt⁶⁴, R. Vértesi¹⁴⁷, M. Verweij⁶⁴, L. Vickovic³⁶, Z. Vilakazi¹³⁴, O. Villalobos Baillie¹¹³, G. Vino⁵⁴, A. Vinogradov⁹¹, T. Virgili³⁰, V. Vislavicius⁹², A. Vodopyanov⁷⁷, B. Volkel³⁵, M.A. Völkl¹⁰⁷, K. Voloshin⁹⁵, S.A. Voloshin¹⁴⁵, G. Volpe³⁴, B. von Haller³⁵, I. Vorobyev¹⁰⁸, D. Voscek¹¹⁹, N. Vozniuk⁶⁵, J. Vrláková³⁹, B. Wagner²¹, C. Wang⁴¹, D. Wang⁴¹, M. Weber¹¹⁶, A. Wegrzynek³⁵, S.C. Wenzel³⁵, J.P. Wessels¹⁴⁶, J. Wiechula⁷⁰, J. Wikne²⁰, G. Wilk⁸⁸, J. Wilkinson¹¹⁰, G.A. Willems¹⁴⁶, B. Windelband¹⁰⁷, M. Winn¹⁴⁰, W.E. Witt¹³³, J.R. Wright¹²¹, W. Wu⁴¹, Y. Wu¹³¹, R. Xu⁷, A.K. Yadav¹⁴³, S. Yalcin⁷⁹, Y. Yamaguchi⁴⁷, K. Yamakawa⁴⁷, S. Yang²¹, S. Yano⁴⁷, Z. Yin⁷, H. Yokoyama⁶⁴, I.-K. Yoo¹⁷, J.H. Yoon⁶³, S. Yuan²¹, A. Yuncu¹⁰⁷, V. Zaccolo²⁴, A. Zaman¹⁴, C. Zampolli³⁵, H.J.C. Zanolli⁶⁴, N. Zardoshti³⁵, A. Zarochentsev¹¹⁵, P. Závada⁶⁸, N. Zaviyalov¹¹¹, M. Zhalov¹⁰¹, B. Zhang⁷, S. Zhang⁴¹, X. Zhang⁷, Y. Zhang¹³¹, V. Zherebchevskii¹¹⁵, Y. Zhi¹¹, N. Zhigareva⁹⁵, D. Zhou⁷, Y. Zhou⁹², J. Zhu^{7,110}, Y. Zhu⁷, A. Zichichi²⁶, G. Zinovjev³, N. Zurlo^{142,59}

Affiliation notes

^I Deceased

^{II} Also at: Italian National Agency for New Technologies, Energy and Sustainable Economic Development (ENEA), Bologna, Italy

^{III} Also at: Dipartimento DET del Politecnico di Torino, Turin, Italy

^{IV} Also at: M.V. Lomonosov Moscow State University, D.V. Skobeltsyn Institute of Nuclear, Physics, Moscow, Russia

^V Also at: Department of Applied Physics, Aligarh Muslim University, Aligarh, India

^{VI} Also at: Institute of Theoretical Physics, University of Wrocław, Poland

Collaboration Institutes

¹ A.I. Alikhanyan National Science Laboratory (Yerevan Physics Institute) Foundation, Yerevan, Armenia

² AGH University of Science and Technology, Cracow, Poland

³ Bogolyubov Institute for Theoretical Physics, National Academy of Sciences of Ukraine, Kiev, Ukraine

⁴ Bose Institute, Department of Physics and Centre for Astroparticle Physics and Space Science (CAPSS), Kolkata, India

⁵ Budker Institute for Nuclear Physics, Novosibirsk, Russia

⁶ California Polytechnic State University, San Luis Obispo, California, United States

- ⁷ Central China Normal University, Wuhan, China
- ⁸ Centro de Aplicaciones Tecnológicas y Desarrollo Nuclear (CEADEN), Havana, Cuba
- ⁹ Centro de Investigación y de Estudios Avanzados (CINVESTAV), Mexico City and Mérida, Mexico
- ¹⁰ Chicago State University, Chicago, Illinois, United States
- ¹¹ China Institute of Atomic Energy, Beijing, China
- ¹² Chungbuk National University, Cheongju, Republic of Korea
- ¹³ Comenius University Bratislava, Faculty of Mathematics, Physics and Informatics, Bratislava, Slovakia
- ¹⁴ COMSATS University Islamabad, Islamabad, Pakistan
- ¹⁵ Creighton University, Omaha, Nebraska, United States
- ¹⁶ Department of Physics, Aligarh Muslim University, Aligarh, India
- ¹⁷ Department of Physics, Pusan National University, Pusan, Republic of Korea
- ¹⁸ Department of Physics, Sejong University, Seoul, Republic of Korea
- ¹⁹ Department of Physics, University of California, Berkeley, California, United States
- ²⁰ Department of Physics, University of Oslo, Oslo, Norway
- ²¹ Department of Physics and Technology, University of Bergen, Bergen, Norway
- ²² Dipartimento di Fisica dell'Università 'La Sapienza' and Sezione INFN, Rome, Italy
- ²³ Dipartimento di Fisica dell'Università and Sezione INFN, Cagliari, Italy
- ²⁴ Dipartimento di Fisica dell'Università and Sezione INFN, Trieste, Italy
- ²⁵ Dipartimento di Fisica dell'Università and Sezione INFN, Turin, Italy
- ²⁶ Dipartimento di Fisica e Astronomia dell'Università and Sezione INFN, Bologna, Italy
- ²⁷ Dipartimento di Fisica e Astronomia dell'Università and Sezione INFN, Catania, Italy
- ²⁸ Dipartimento di Fisica e Astronomia dell'Università and Sezione INFN, Padova, Italy
- ²⁹ Dipartimento di Fisica e Nucleare e Teorica, Università di Pavia, Pavia, Italy
- ³⁰ Dipartimento di Fisica 'E.R. Caianiello' dell'Università and Gruppo Collegato INFN, Salerno, Italy
- ³¹ Dipartimento DISAT del Politecnico and Sezione INFN, Turin, Italy
- ³² Dipartimento di Scienze e Innovazione Tecnologica dell'Università del Piemonte Orientale and INFN Sezione di Torino, Alessandria, Italy
- ³³ Dipartimento di Scienze MIFT, Università di Messina, Messina, Italy
- ³⁴ Dipartimento Interateneo di Fisica 'M. Merlin' and Sezione INFN, Bari, Italy
- ³⁵ European Organization for Nuclear Research (CERN), Geneva, Switzerland
- ³⁶ Faculty of Electrical Engineering, Mechanical Engineering and Naval Architecture, University of Split, Split, Croatia
- ³⁷ Faculty of Engineering and Science, Western Norway University of Applied Sciences, Bergen, Norway
- ³⁸ Faculty of Nuclear Sciences and Physical Engineering, Czech Technical University in Prague, Prague, Czech Republic
- ³⁹ Faculty of Science, P.J. Šafárik University, Košice, Slovakia
- ⁴⁰ Frankfurt Institute for Advanced Studies, Johann Wolfgang Goethe-Universität Frankfurt, Frankfurt, Germany
- ⁴¹ Fudan University, Shanghai, China
- ⁴² Gangneung-Wonju National University, Gangneung, Republic of Korea
- ⁴³ Gauhati University, Department of Physics, Guwahati, India
- ⁴⁴ Helmholtz-Institut für Strahlen- und Kernphysik, Rheinische Friedrich-Wilhelms-Universität Bonn, Bonn, Germany
- ⁴⁵ Helsinki Institute of Physics (HIP), Helsinki, Finland
- ⁴⁶ High Energy Physics Group, Universidad Autónoma de Puebla, Puebla, Mexico
- ⁴⁷ Hiroshima University, Hiroshima, Japan
- ⁴⁸ Hochschule Worms, Zentrum für Technologietransfer und Telekommunikation (ZTT), Worms, Germany
- ⁴⁹ Horia Hulubei National Institute of Physics and Nuclear Engineering, Bucharest, Romania
- ⁵⁰ Indian Institute of Technology Bombay (IIT), Mumbai, India
- ⁵¹ Indian Institute of Technology Indore, Indore, India
- ⁵² Indonesian Institute of Sciences, Jakarta, Indonesia
- ⁵³ INFN, Laboratori Nazionali di Frascati, Frascati, Italy
- ⁵⁴ INFN, Sezione di Bari, Bari, Italy
- ⁵⁵ INFN, Sezione di Bologna, Bologna, Italy
- ⁵⁶ INFN, Sezione di Cagliari, Cagliari, Italy
- ⁵⁷ INFN, Sezione di Catania, Catania, Italy
- ⁵⁸ INFN, Sezione di Padova, Padova, Italy

- 59 INFN, Sezione di Pavia, Pavia, Italy
- 60 INFN, Sezione di Roma, Rome, Italy
- 61 INFN, Sezione di Torino, Turin, Italy
- 62 INFN, Sezione di Trieste, Trieste, Italy
- 63 Inha University, Incheon, Republic of Korea
- 64 Institute for Gravitational and Subatomic Physics (GRASP), Utrecht University/Nikhef, Utrecht, Netherlands
- 65 Institute for Nuclear Research, Academy of Sciences, Moscow, Russia
- 66 Institute of Experimental Physics, Slovak Academy of Sciences, Košice, Slovakia
- 67 Institute of Physics, Homi Bhabha National Institute, Bhubaneswar, India
- 68 Institute of Physics of the Czech Academy of Sciences, Prague, Czech Republic
- 69 Institute of Space Science (ISS), Bucharest, Romania
- 70 Institut für Kernphysik, Johann Wolfgang Goethe-Universität Frankfurt, Frankfurt, Germany
- 71 Instituto de Ciencias Nucleares, Universidad Nacional Autónoma de México, Mexico City, Mexico
- 72 Instituto de Física, Universidade Federal do Rio Grande do Sul (UFRGS), Porto Alegre, Brazil
- 73 Instituto de Física, Universidad Nacional Autónoma de México, Mexico City, Mexico
- 74 iThemba LABS, National Research Foundation, Somerset West, South Africa
- 75 Jeonbuk National University, Jeonju, Republic of Korea
- 76 Johann-Wolfgang-Goethe Universität Frankfurt Institut für Informatik, Fachbereich Informatik und Mathematik, Frankfurt, Germany
- 77 Joint Institute for Nuclear Research (JINR), Dubna, Russia
- 78 Korea Institute of Science and Technology Information, Daejeon, Republic of Korea
- 79 KTO Karatay University, Konya, Turkey
- 80 Laboratoire de Physique des 2 Infinis, Irène Joliot-Curie, Orsay, France
- 81 Laboratoire de Physique Subatomique et de Cosmologie, Université Grenoble-Alpes, CNRS-IN2P3, Grenoble, France
- 82 Lawrence Berkeley National Laboratory, Berkeley, California, United States
- 83 Lund University Department of Physics, Division of Particle Physics, Lund, Sweden
- 84 Moscow Institute for Physics and Technology, Moscow, Russia
- 85 Nagasaki Institute of Applied Science, Nagasaki, Japan
- 86 Nara Women's University (NWU), Nara, Japan
- 87 National and Kapodistrian University of Athens, School of Science, Department of Physics, Athens, Greece
- 88 National Centre for Nuclear Research, Warsaw, Poland
- 89 National Institute of Science Education and Research, Homi Bhabha National Institute, Jatni, India
- 90 National Nuclear Research Center, Baku, Azerbaijan
- 91 National Research Centre Kurchatov Institute, Moscow, Russia
- 92 Niels Bohr Institute, University of Copenhagen, Copenhagen, Denmark
- 93 Nikhef, National institute for subatomic physics, Amsterdam, Netherlands
- 94 NRC Kurchatov Institute IHEP, Protvino, Russia
- 95 NRC «Kurchatov»Institute - ITEP, Moscow, Russia
- 96 NRNU Moscow Engineering Physics Institute, Moscow, Russia
- 97 Nuclear Physics Group, STFC Daresbury Laboratory, Daresbury, United Kingdom
- 98 Nuclear Physics Institute of the Czech Academy of Sciences, Řež u Prahy, Czech Republic
- 99 Oak Ridge National Laboratory, Oak Ridge, Tennessee, United States
- 100 Ohio State University, Columbus, Ohio, United States
- 101 Petersburg Nuclear Physics Institute, Gatchina, Russia
- 102 Physics department, Faculty of science, University of Zagreb, Zagreb, Croatia
- 103 Physics Department, Panjab University, Chandigarh, India
- 104 Physics Department, University of Jammu, Jammu, India
- 105 Physics Department, University of Rajasthan, Jaipur, India
- 106 Physikalisches Institut, Eberhard-Karls-Universität Tübingen, Tübingen, Germany
- 107 Physikalisches Institut, Ruprecht-Karls-Universität Heidelberg, Heidelberg, Germany
- 108 Physik Department, Technische Universität München, Munich, Germany
- 109 Politecnico di Bari and Sezione INFN, Bari, Italy
- 110 Research Division and ExtreMe Matter Institute EMMI, GSI Helmholtzzentrum für Schwerionenforschung GmbH, Darmstadt, Germany
- 111 Russian Federal Nuclear Center (VNIIEF), Sarov, Russia

- 112 Saha Institute of Nuclear Physics, Homi Bhabha National Institute, Kolkata, India
- 113 School of Physics and Astronomy, University of Birmingham, Birmingham, United Kingdom
- 114 Sección Física, Departamento de Ciencias, Pontificia Universidad Católica del Perú, Lima, Peru
- 115 St. Petersburg State University, St. Petersburg, Russia
- 116 Stefan Meyer Institut für Subatomare Physik (SMI), Vienna, Austria
- 117 SUBATECH, IMT Atlantique, Université de Nantes, CNRS-IN2P3, Nantes, France
- 118 Suranaree University of Technology, Nakhon Ratchasima, Thailand
- 119 Technical University of Košice, Košice, Slovakia
- 120 The Henryk Niewodniczanski Institute of Nuclear Physics, Polish Academy of Sciences, Cracow, Poland
- 121 The University of Texas at Austin, Austin, Texas, United States
- 122 Universidad Autónoma de Sinaloa, Culiacán, Mexico
- 123 Universidade de São Paulo (USP), São Paulo, Brazil
- 124 Universidade Estadual de Campinas (UNICAMP), Campinas, Brazil
- 125 Universidade Federal do ABC, Santo Andre, Brazil
- 126 University of Cape Town, Cape Town, South Africa
- 127 University of Houston, Houston, Texas, United States
- 128 University of Jyväskylä, Jyväskylä, Finland
- 129 University of Kansas, Lawrence, Kansas, United States
- 130 University of Liverpool, Liverpool, United Kingdom
- 131 University of Science and Technology of China, Hefei, China
- 132 University of South-Eastern Norway, Tonsberg, Norway
- 133 University of Tennessee, Knoxville, Tennessee, United States
- 134 University of the Witwatersrand, Johannesburg, South Africa
- 135 University of Tokyo, Tokyo, Japan
- 136 University of Tsukuba, Tsukuba, Japan
- 137 Université Clermont Auvergne, CNRS/IN2P3, LPC, Clermont-Ferrand, France
- 138 Université de Lyon, CNRS/IN2P3, Institut de Physique des 2 Infinis de Lyon, Lyon, France
- 139 Université de Strasbourg, CNRS, IPHC UMR 7178, F-67000 Strasbourg, France, Strasbourg, France
- 140 Université Paris-Saclay Centre d'Etudes de Saclay (CEA), IRFU, Département de Physique Nucléaire (DPhN), Saclay, France
- 141 Università degli Studi di Foggia, Foggia, Italy
- 142 Università di Brescia, Brescia, Italy
- 143 Variable Energy Cyclotron Centre, Homi Bhabha National Institute, Kolkata, India
- 144 Warsaw University of Technology, Warsaw, Poland
- 145 Wayne State University, Detroit, Michigan, United States
- 146 Westfälische Wilhelms-Universität Münster, Institut für Kernphysik, Münster, Germany
- 147 Wigner Research Centre for Physics, Budapest, Hungary
- 148 Yale University, New Haven, Connecticut, United States
- 149 Yonsei University, Seoul, Republic of Korea